AD-A165 276 A SURVEY OF KNOWN INDICATORS OF AURORAL SUBSTORM ONSET 1/1
(U) AIR FORCE GEOPHYSICS LAB HANSCOM AFB MA J O WISE
29 AUG 85 AFGL-TR-85-0197

UNCLASSIFIED F/G 4/1 NL

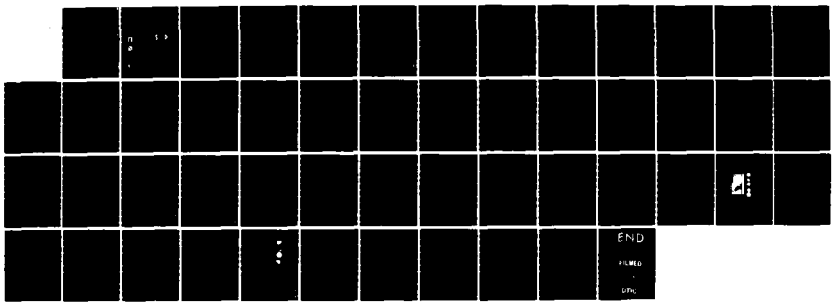

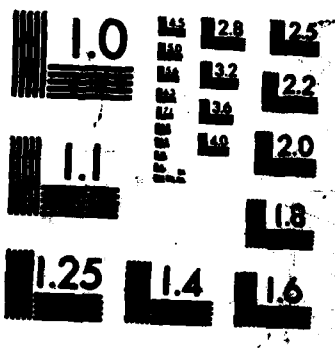

(12)

AFGL-TR-85-0197
ENVIRONMENTAL RESEARCH PAPERS, NO. 928

A Survey of Known Indicators of Auroral Substorm Onset

JOHN O. WISE

29 August 1985

CIRRIS 1A PROGRAM OFFICE
PROJECT 5321
AIR FORCE GEOPHYSICS LABORATORY
HANSCOM AFB, MA 01731

"This technical report has been reviewed and is approved for publication"

FOR THE COMMANDER

RICHARD NADILE
CIRRIS-1A Sciences Branch

LAWRENCE L VANDIFORD, Major, USAF
CIRRIS-1A Program Manager

This report has been reviewed by the ESD Public Affairs Office (PA) and is releasable to the National Technical Information Services (NTIS).

Qualified requestors may obtain additional copies from the Defense Technical Information Center. All others should apply to the National Technical Information Center.

If your address has changed, or if you wish to be removed from the mailing list, or if the addressee is no longer employed by your organization, please notify AFGL/DAA, Hanscom AFB, MA 01731. This will assist us in maintaining a current mailing list.

DISCLAIMER NOTICE

THIS DOCUMENT IS BEST QUALITY PRACTICABLE. THE COPY FURNISHED TO DTIC CONTAINED A SIGNIFICANT NUMBER OF PAGES WHICH DO NOT REPRODUCE LEGIBLY.

Unclassified

SECURITY CLASSIFICATION OF THIS PAGE

REPORT DOCUMENTATION PAGE

1a. REPORT SECURITY CLASSIFICATION: Unclassified	1b. RESTRICTIVE MARKINGS
2a. SECURITY CLASSIFICATION AUTHORITY	3. DISTRIBUTION/AVAILABILITY OF REPORT: Approved for public release; Distribution unlimited.
2b. DECLASSIFICATION/DOWNGRADING SCHEDULE	
4. PERFORMING ORGANIZATION REPORT NUMBER(S): AFGL-TR-85-0197 ERP, No. 926	5. MONITORING ORGANIZATION REPORT NUMBER(S)
6a. NAME OF PERFORMING ORGANIZATION: Air Force Geophysics Laboratory; 6b. OFFICE SYMBOL (If applicable): CMS	7a. NAME OF MONITORING ORGANIZATION
6c. ADDRESS (City, State and ZIP Code): Hanscom AFB Massachusetts 01731	7b. ADDRESS (City, State and ZIP Code)
8a. NAME OF FUNDING/SPONSORING ORGANIZATION; 8b. OFFICE SYMBOL (If applicable)	9. PROCUREMENT INSTRUMENT IDENTIFICATION NUMBER
8c. ADDRESS (City, State and ZIP Code)	10. SOURCE OF FUNDING NOS.

PROGRAM ELEMENT NO.	PROJECT NO.	TASK NO.	WORK UNIT NO.
63220C	5321	05	66

11. TITLE (Include Security Classification) A Survey of Known Indicators of Auroral Substorm Onset

12. PERSONAL AUTHOR(S) John O. Wise

13a. TYPE OF REPORT	13b. TIME COVERED	14. DATE OF REPORT (Yr., Mo., Day)	15. PAGE COUNT
Research	FROM 1 Jan TO 9 May	85 1985 August 29	50

16. SUPPLEMENTARY NOTATION

17 COSATI CODES			18. SUBJECT TERMS (Continue on reverse if necessary and identify by block number)
FIELD	GROUP	SUB. GR.	Auroral substorm prediction; Substorm onset; Equatorward boundary.

19. ABSTRACT (Continue on reverse if necessary and identify by block number)

This report summarizes current research in the area of auroral substorm prediction. Long term indicators are investigated; in particular the solar cycle solar flares coronal holes, and the tendency for these phenomena to recur. Short term indicators are also reviewed: recurrence probability in DMSP images, the solar winds and the interplanetary magnetic field, the equatorward boundary of the auroral oval, electron density dropouts at geosynchronous orbit, visual observations from the ground, magnetometers measurements, auroral radar and riometer measurements. Keywords: Defense Meteorological Satellite Program

20. DISTRIBUTION/AVAILABILITY OF ABSTRACT	21. ABSTRACT SECURITY CLASSIFICATION
UNCLASSIFIED/UNLIMITED ☒ SAME AS RPT. ☐ DTIC USERS ☐	Unclassified

22a. NAME OF RESPONSIBLE INDIVIDUAL	22b. TELEPHONE NUMBER (Include Area Code)	22c. OFFICE SYMBOL
John O. Wise	(617) 861-4428	CMS

DD FORM 1473, 83 APR EDITION OF 1 JAN 73 IS OBSOLETE.

Unclassified

SECURITY CLASSIFICATION OF THIS PAGE

Contents

Illustrations

Tables

A Survey of Known Indicators of Auroral Substorm Onset

I. INTRODUCTION

The study of when and where auroral phenomena will occur has become an area of major concern, particularly in recent years. As scientists learn more about the mechanisms for various auroral emissions through repeated measurements, the measurements themselves have become increasingly more refined. As the interest in the more subtle emissions increases, scientists are seeking to measure intense discrete auroral emissions of Class III aurorae or greater.

Early ground observations usually involved little more than a knowledge of periodic solar activity and ground based magnetometer variations. Once a substorm commences it can be immediately measured from the ground. The evolvement to more complicated airborne measurements requires extensive planning, both in the long term, due to increased costs, and in the short term, due to delays between launching the vehicle and acquiring the often erratic auroral event.

Short term predictions are useful for experiments on vehicles capable of dynamic measurements such as the space shuttle, which may prove to be one of the most effective vehicles for auroral acquisition. The shuttle has the capability of accessing large sections of the auroral zone from an altitude of approximately 200-400 km. Given indications within 30 min as to the region for the highest likelihood of auroral occurrence, the orbiter can be oriented such that it could acquire the auroral event.

(Received for publication 26 August 1985)

The approach of this report will be to discuss two kinds of auroral indicators. The first section discusses long term indicators. These involve solar events such as the sunspot cycle, solar flares and coronal holes. Observations of this type usually involve lead times of one day to approximately eleven years.

The second section discusses short term indicators, with lead times ranging from instantaneous to an hour or so before substorm onset. These indicators involve satellites and ground measurements. There are periodic measurements of the auroral oval by low orbiting (~800 km) satellites that pass over roughly the same geomagnetic zone once every 102 minutes. They show the location of the equatorward boundary of the oval and the general level of substorm activity in the oval. In addition there are higher satellites at geosynchronous orbits (about 6.6 earth radii) which can measure particle flux densities and magnetic fields, and even higher satellites which can measure the intensity of the interplanetary magnetic field in the bowshock region outside the magnetosphere towards the sun. (There are no such operational satellites in this region in the present year, 1985.) Ground based measurements, such as all sky visual observations and magnetograms, are useful for tracking the phase of the substorm.

2. LONG TERM INDICATORS

2.1 The 11-Year Sunspot Cycle and the 27-Day Recurrence Tendency

All considerations for the source of auroral electrons and protons begin with the sun. Observations of sunspot activity have indicated a definite periodicity of eleven years. This period is called the sunspot cycle. During the cycle, sunspot activity generally rises to a maximum and then subsides. It is between the maximum and the end of the cycle when auroral activity is known to be highest. According to Chamberlain[1] it is about two years after this sunspot maximum. But recent studies by Gneryshev[2] have indicated that the maximum is actually the first of two maxima, the second of which occurs about two to three years after the first. Gneryshev characterizes the first maxima by a maximum number of small sunspots and flares, a homogeneous corona, and few auroral occurrences. The second maxima is characterized by bigger sunspots and flares, a very inhomogeneous corona, and a maximum number of auroral occurrences.

---

1. Chamberlain, J.W. (1961) Physics of the Aurora and Airglow, Academic Press, New York.
2. Gneryshev, M.N. (1977) Essential features of the 11-year solar cycle, Solar Physics, 51:175-183.

The sun rotates with respect to the earth once every 27 days. Sources of high speed streams in the solar wind on the sun's surface tend to rotate as rigid volumes with only a very slight variation of their rotational period with latitude.[3] Hence there is a tendency for the effects of these sources to repeat every 27 days. Musical diagrams of the Kp index are sometimes suggestive of this recurrence tendency, depending on the stage of the sunspot cycle. One such diagram is shown in Figure 1 (after Mayaud[4]) for the year 1933 when recurrence was high.

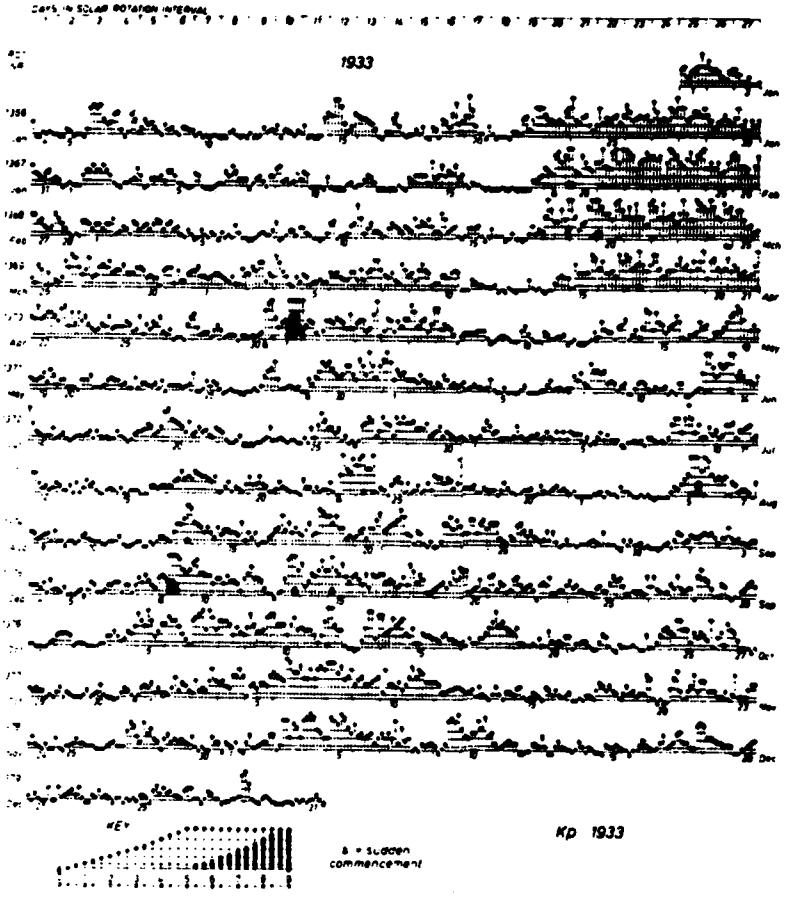

Figure 1. A 'Musical' Kp Diagram

3. Timothy, A. F., Krieger, A.S., and Vaiana, G.S. (1975) Solar Physics, 42:135.
4. Mayaud, P. N. (1980) Derivation, meaning and use of geomagnetic indices, American Geophysical Union, Geophysical Monograph 22, Washington, D.C.

Sargent[2] has combined the 27-day recurrence phenomenon in the aa index (instead of Kp) with the overall periodicity of the sunspot cycle every 11 years, the results of which are shown in Figure 2. The aa index is based upon the basic K indices and is probably one of the best indicators of long term geomagnetic activity based on the homogeneity of the series and the indices' reliability as a worldwide indicator.[6] In his analysis Sargent[5] has computed a correlation coefficient by matching a set of 54 aa indices for a 27-day rotation with the set of 54 aa indices for the next 27-day rotation and assigned this correlation coefficient for the whole 54-day period.

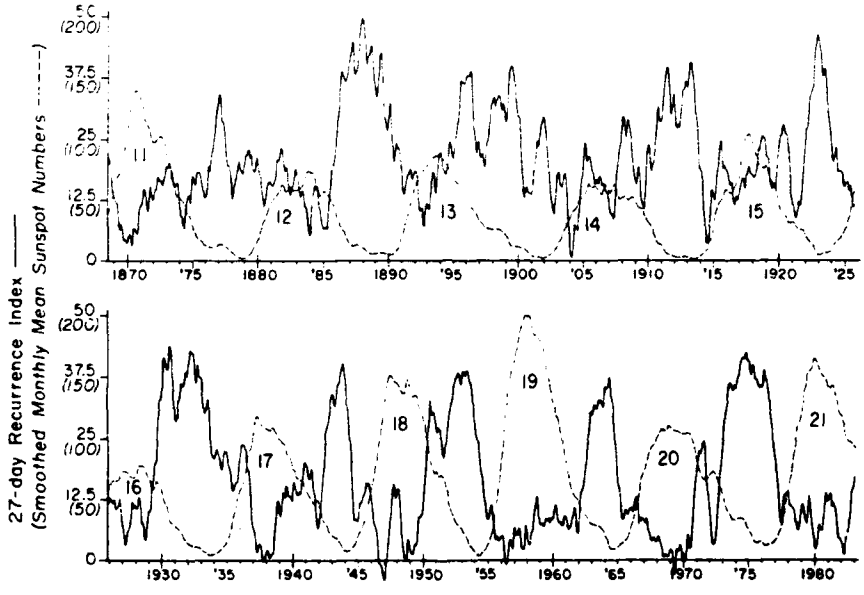

Figure 2. Twenty-Seven-Day Recurrence Index (solid line) and Smoothed Monthly Mean Sunspot Numbers (dashed line) From 1968 to Present. Sunspot cycles are numbered according to convention

He noted the following features in the trends of recurrent activity:

(1) The onset of the recurrent activity is usually abrupt, and for much of the past 116 years it is possible to say confidently whether or not the signal is present.

---

5. Sargent, H.H. (1985) Recurrent geomagnetic activity: evidence for long-lived stability in solar wind structure, J. Geophys. Res., 90:1425-1428.

6. Mayaud, P.N. (1973) A hundred year series of geomagnetic data 1868-1967, IAGA Bull. Vol. 33.

(2) The termination of the recurrent period is almost always as abrupt as the onset and occurs about 1 year into the new sunspot cycle.

(3) The duration of the recurrent phases is longer in some cycles than in others. These longer phases occur every 22 years. The lengths of these periods of recurrent behavior are surprisingly long, accounting, at times, for as much as 5 years of a sunspot cycle.[5]

2.2 Coronal Holes

Coronal holes are regions of unusually low density and low temperature in the solar corona. It has generally been accepted that the 27-day recurrent behavior is directly related to these open field structures on the sun,[7] which are sources of high speed streams in the solar wind. This acceptance has been based upon observations that long lived patterns of coronal holes, high speed solar wind streams, and geomagnetic disturbances appear remarkably alike. Sheeley has noticed that the polarity of the magnetic field emerging from the base of a coronal hole is the same as the predominant polarity of the interplanetary magnetic field carried by the corresponding high speed stream.[8]

Sheeley found the transit time from passage of the coronal hole over the sun's central meridian to the time of geomagnetic disturbance to be about 2.5 days, assuming the latitude of the hole is close to the heliographic latitude of the earth. However, this is only an average figure. Sometimes the streams arrive at the earth before the hole's central meridian passage or after. This may be due to the fact that the boundaries of coronal holes sometimes extend non-radially from their bases in the chromosphere into the outer corona. Koomen[9] also deduced from satellite measurements at 3-10 Re that photospheric magnetic flux emerging from low latitudinal coronal holes may fan out considerably with distance from the sun. Sheeley suggests the low latitude flux could join with flux from a polar coronal hole to form a large scale interplanetary magnetic sector. He concludes that "since coronal holes are visible from the earth several days before they are carried across the central meridian by solar rotation, and since 2-3 days remain before the wind from the hole would reach the earth, we should expect to be able to predict the arrival of the high speed streams and their associated magnetic effects approximately a week in advance."

---

7. Suess, S.T. (1979) Models of coronal hole flows, Space Science Review, 23:159-200.
8. Sheeley, N.R., Harvey, J.W., and Feldman, W.C. (1976) Coronal holes, solar wind streams, and recurrent geomagnetic disturbances: 1973-1976, Solar Physics, 49:271-278.
9. Koomen, M.J., and Howard, R.A. (1974) Solar Physics, 37:469.

2.3 Solar Flares

A solar flux is a sudden brightening of the photosphere that remains visible for several hours. Solar flares tend to occur near sunspots and their number can be related to the number of sunspots[10] by

$$N_f = \alpha(\bar{R} - 10) .$$

Where N_f is the number of flares per solar rotation, $\bar{R}$ is the mean sunspot number and α is a constant value between 1.5 and 2.

The most spectacular aurorae are usually associated with solar flares.[1] Newton[11] found that the largest flares, when they occurred within 45° of the center of the disk, were followed in 80 percent of the cases by a magnetic storm within a maximum time of three days. The most likely time interval between a great flare and its associated magnetic storm is about one day or slightly less,[12] but many occur one to two days after the event. Generally, stronger flares have shorter lead times before the substorm onset than the lead times of weaker flares.

Dodson and Hederman[13] showed that a flare was especially effective (92 percent of the cases studied) if it is accompanied by solar radio bursts below 200 Mhz before the flare reaches maximum brightness.

Krivsky[14] did a similar study but only analyzed solar radio bursts at the frequencies of 536 and 606 MHz, and with 200 solar flux units (solar flux unit = $10\ W^{-22}\ m^{-2}\ Hz^{-1}$). Krivsky first compared proton flare occurrence with Ae index levels for 32 superimposed epochs. The patterns showed a rise in the Ae index beginning three days prior to the flare event and peaking on the second day after the flare, followed by a decrease. A similar analysis of the radio bursts at 536 and 606 MHz indicated the Ae index rose 3 to 4 days prior to the burst and peaked 6 to 8 days after the burst. Krivsky concluded that a rise in the Ae index could be associated with an active sunspot region where multiple non-proton radio bursts occurring before and after the flare accounted for a rise in the average Ae index value to a noise level of about 230 gamma prior to and after an enhanced peak from a major flare event. These results are shown in Figure 3.

(Due to the large number of references cited above, they will not be listed here. See References, page 39.)

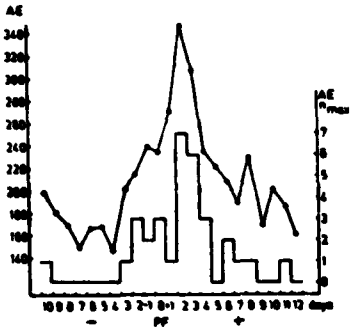

Figure 3a. Curve of the Average Values of the AE Index 10 Days Prior to the Occurrence of the Proton Flare (flare day = 0) and 12 Days After the Occurrence. The left-hand scale is in units of γ. Number of superimposed epochs: 32. The interval of years 1966-1973. The curve of the hisotrogram on the same graph gives the numbers of occurrences of the maxima of the AE index in the interval -10 to +12 days, pertinent to the individual epochs employed (numbers scale on the right)

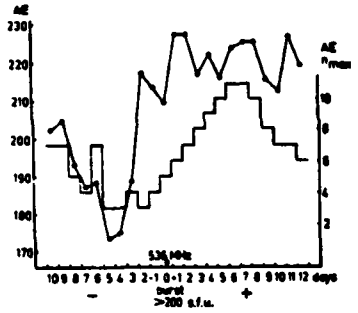

Figure 3b. Curve of the Average Values of the AE Index 10 Days Prior to and 12 Days After the Occurrence of the Solar Radio Burst With a Flux in Excess of 200 s.f.u. (solar flux unit = $10\ W^{-22}\ m^{-2}\ Hz^{-1}$ on a Frequency of 536 MHz (Ondrejov Observatory). Number of epochs 152, in years 1966-1973. Left-hand scale is in units of γ. The curve of the histogram also gives the numbers of occurrences of the maxima of the AE index on the individual days (right-hand scale), the data being adopted from the individual epochs employed

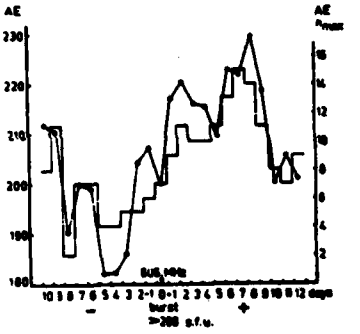

Figure 3c. Curve of the Average Values of the AE Index 10 Days Prior and 12 Days After the Occurrence of the Solar Radio Burst With a Flux in Excess of 200 s.f.u. on a Frequency of 606 MHz (Sagamore Hill Observatory). Number of epochs: 120 from interval of years 1966-1973. Left-hand scale is in units of γ. The curve of the histogram gives the number of occurrences of the maxima of the AE index on the individual days (right-hand scale), the data being adopted from the individual epochs employed

3. SHORT TERM INDICATORS

3.1 Recurrence Probability of Auroral Activity in DMSP Images

Much has been learned about the auroral oval from the DMSP satellites, which scan a path approximately 3000 km wide on the earth's surface. The altitude of the satellites is about 800 km. The mapping takes into account a very large portion of the auroral oval so that a fair evaluation can be given to the level of auroral activity and the latitudinal extent of the oval. Sheehan et al[15] rated 749 southern hemispheric DMSP images taken during 1972 and 1973 and rated them according to active (A), moderate (M), quiet (Q) and no aurora (N), finding the overall occurrence rates of each to be 0.17, 0.55, 0.16, and 0.11 respectively for those years. He also found that after one DMSP orbit both A and Q tended to recur in one-half of the cases. As a result there was some doubt cast on Akasofu's early substorm model[16] since Sheehan concluded that it was possible for magnetic bays of several hours to occur.[17] In Figure 4, Sheehan[18] geographically shows an example of how the entire oval substorm should be considered in the determination of magnetic bay deviations rather than by the duration of a bay at a particular station, stating "The magnetic signature at a fixed location on earth develops as the earth rotates under an essentially stationary auroral pattern."[3]

Sheehan[18] has tabulated the number of occurrences of the A, M, Q, N, and X (missing data) ratings with respect to the rating from the previous pass and has constructed a matrix called a persistence table.

Two such tables are shown in Table 1 and Table 2. Sheehan's persistence tables indicated significant likelihood for activity levels to recur on the next pass 102 min later.

---

15. Sheehan, R.E., Carovillano, R.L., and Gussenhoven, M.S. (1982) Occurrence and recurrence in auroral activity in DMSP images, J. Geophys. Res., 87(No. A3):3581-3589.
16. Akasofu, S.-I. (1968) Polar and Magnetospheric Substorms, D. Reidel, Hingham, Massachusetts.
17. Carovillano, R.L., Siscoe, G.L., Sheehan, R.E., Eather, R.H., and Gussenhoven, M.S. (1975) Unified Model of Auroral Substorm Development, AFCRL-TR-75-0558, AD A020313.
18. Sheehan, R.E. Ph. D. Thesis (Boston College, 1977), p. 182.

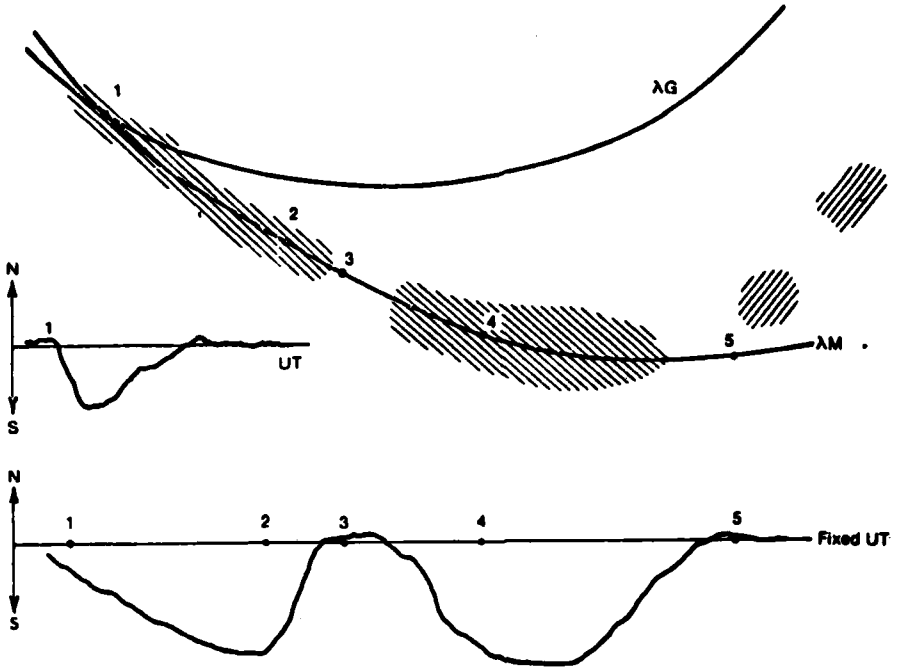

Figure 4. Schematic Representation of the Relationship of Magnetic Bay Activity and Overhead Aurora. λ_G and λ_M denote lines of constant geographic and geomagnetic latitude, respectively. The shaded zones denote areas of active aurora in a DMSP image. The upper inset gives the horizontal (N-S) component of the magnetic field at Station I as it rotates in UT under the aurora. The lower inset traces the horizontal component of the magnetic field along λ_M at the fixed UT which applies to the DMSP image (after Sheehan, 1977)

In addition Sheehan has developed a scheme for computing the probability that an image rating will be followed by the same or another image rating for any number of orbits later. Defining P_{ij} to be the occurrence frequency of an image rated at index j to be immediately followed by one of index i, the joint probability that an image of index j is followed by one of index i two orbits later is given by

$$P_{ij}^{2} = \sum_{k} P_{ik} P_{kj}$$

Table 1. Persistence Table for August 1972. Elements in table give the number of cases and percentage (in parentheses) that images with a chosen rating (column) were followed by images with the same or any other rating one orbit later (row). For example, the element 9(18) in column A, row M indicates that 9 images (18 %) of the 49 rated A in August 1972 were followed by M rated images one orbit later (after Sheehan, 1977)[18]

	August 1972					
	A	M+	M	M-	Q	N
A	20(41)	9(27)	7(15)	5(11)	2(04)	2(05)
M+	7(14)	5(15)	8(17)	3(07)	3(05)	0(00)
M	9(18)	9(27)	8(17)	5(11)	7(13)	3(07)
M-	5(10)	3(09)	7(15)	9(20)	7(13)	3(07)
Q	3(06)	3(09)	7(15)	12(27)	9(16)	9(21)
N	0(00)	2(06)	1(02)	3(07)	8(15)	16(37)
X	5(10)	2(06)	9(19)	7(16)	19(35)	10(23)
Total	49(100)	33(100)	47(100)	44(100)	55(100)	43(100)

Table 2. Combined Persistence Table Based on All Images (748) in August 1972 and July - August 1973 (after Sheehan, 1977)[18]

	Combined					
	A	M+	M	M-	Q	N
A	52(50)	20(24)	26(14)	5(04)	4(03)	2(02)
M+	23(18)	9(11)	21(11)	3(02)	3(02)	0(00)
M	19(15)	26(31)	61(32)	23(17)	14(11)	4(05)
M-	6(05)	6(07)	22(11)	32(24)	21(17)	8(10)
Q	4(03)	3(04)	19(10)	30(22)	19(15)	13(16)
N	0(00)	2(02)	6(03)	9(07)	15(12)	25(30)
X	27(21)	17(20)	37(19)	34(25)	47(38)	31(37)
Total	131(100)	83(100)	192(100)	136(100)	123(100)	83(100)

The indexing process is diagrammatically shown in Figure 5.

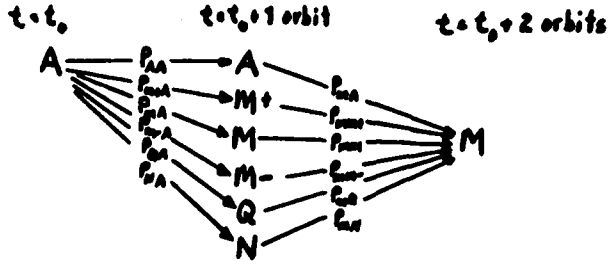

Figure 5. Sheehan, Ph. D. Thesis, (1977)[18]

The procedure can be generalized for any number of orbits (n)

$$P_{ik}^{n} = \sum_{j} P_{ij} P_{jk}^{n-1} .$$

If the process is extended to enough orbits the persistence characteristics would eventually, at least for the data set for 1972-1973, return to the overall recurrence frequencies; namely, A = 0.17, M = 0.55, Q = 0.16 and N = 0.11

For experimental purposes the initiation of the construction of a persistence table perhaps a month or more in advance of a high altitude auroral measurement experiment could be a useful tool in the evaluation of the persistence of substorm activity, since the overall activity would be dependent on recent solar activity.

3.2 The Solar Wind and the Interplanetary Magnetic Field

It was first suggested by Dungey[19] that a southward turning of the interplanetary magnetic field (IMF) between the sun and the earth might affect levels of geomagnetic activity and various solar wind parameters such as the wind velocity, the southward component of the IMF (B_z), and the total strength of the IMF (B). Table 3 shows some analytical expressions, consisting of these parameters, which correlate fairly well with geomagnetic activity. Eather[20] however, has warned

19. Dungey, J.W. (1961) Interplanetary magnetic field and the auroral zones, Phys. Rev. Letters, 6:47.

20. Eather, R.H., Mende, S.B., and Weber, E.J. (1979) Dayside aurora and relevance to substorm current systems and dayside merging, J. Geophys. Res., 84:3339.

that direct correlation of geomagnetic activity with B_z can be misleading; he suggests that B_z changes are not the causative driving mechanism but that sustained periods of negative B_z ($\geq$ 1 hour) increased the probability of substorms. Eather[21] has found better correlation of Ae with the dayside cusp equatorward boundary (directly associated with substorm activity) than with B_z (see Figure 6). The accuracy of the Ae index as a measure of substorm activity is about 0.7 according to Kamide[22] (see Figure 6). The time of increased probable onset of a substorm from the time the solar wind impacts the magnetosphere has been estimated to be about one hour by Kamide,[22] although Baker et al[23] and Meng[24] thought it to be more like 40 minutes.

Table 3. List of the Correlation Studies Between Geomagnetic Indices and Solar Wind Parameters

Author(s)	Geomagnetic index (time resolution)		Relation with solar wind parameters
Snyder *et al.* (1963)[25]	ΣKp	(24 hr)	$\Sigma Kp = (V - 330)/8.44$
Olbert (1968)[26]	ΣKp	(24 hr)	$\Sigma Kp = (V - 262)/6.3$
Ballif *et al.* (1969)[27]	Kp	(3 hr)	$Kp = 9\left[1 - \exp\left(\frac{-aB_{T,N} - 0.35}{7.70}\right)\right]$
Arnoldy (1971)[28]	AE	(1 hr)	$AE = -0.26(\Sigma B_z\tau)_0 - 0.91(\Sigma B_z\tau)_2 + 0.12P_0$ $= -0.33(\Sigma B_z\tau)_2 + 0.12P_0$
Bobrov (1973)[29]	Kp	(3 hr)	$Kp = f(V, B_z, \Delta B_z)$
Garrett *et al.* (1974)[30] [31]	up, AE	(1 hr)	$up, AE \propto C_1 + C_2V(B_z) + C_3V\sigma$
Murayama and Hakamada (1975)	AE	(1 hr)	$AE = CB_zV^2$
Burton *et al.* (1975)[32]	Dst	(2.5 min)	$\frac{d}{dt}Dst_0 = F(E) - aDst_0$
Crooker *et al.* (1977)[33]	Ap		$Ap = 3.5 \times 10^{-5}\overline{B_z}\overline{V}^2 - 1.9$
Svalgaard (1977)[34]	am	(3 hr)	$am = 6.6q(f, z)\frac{BV_0}{21}\left[\frac{nV_0^2}{105}\right]^{1/3} \times \frac{1.17}{(1 + 3\cos^2\phi)^{2/3}}$
Maezawa (1979)[35]	AL, AU, am	(1 hr)	$AL \propto B^{0.63}V^{2.06}(\sin\theta)^{0.54}$ $AU \propto B^{0.67}B^{1.15}(\sin\theta)^{0.36}$ $am \propto B^{1.03}V^{2.34}(\sin\theta)^{0.37}n^{0.2}$
Holzer and Slavin (1979)[36]	AL	(1 hr)	Rate of erosion $\frac{d\Phi_e}{dt} = 0.2(1.9 \times 10^{10}\text{ cm})B_zV_{sw}(\text{km s}^{-1})$ Rate of return $\frac{d\Phi_r}{dt} = 1.8 \times 10^{10}AL(\gamma)$
Murayama (1979)[37]	AL	(1 hr)	$AL = 60(B_z + 0.5)V^2F(\chi, B_z)n^{0.15}$
Murayama *et al.* (1981)* [38]	AL	(1 hr)	$AL/V^2 = K(B_z + 0.5)$
Baker *et al.* (1981)* [23]	AE	(2.5 min)	VB_z, V^2B, B^2V, etc.
Lei *et al.* (1981)* [39]	Correlation between the interplanetary and magnetospheric electric fields		
Reiff *et al.* (1981)* [40]	Correlation between Φ_{PC} and B_z, ε		
Holzer and Slavin (1982)* [41]	AL		BV^2, B_zV, B_z^2V
Iijima and Potemra (1982)* [42]	Correlation between field-aligned current density and VB_z, V^2B, B^2V, etc.		
Meloni *et al.* (1982)* [43]	AE		B_z, VB_z, ε

Note: For details of the expressions and definitions of each notation, see the references in Akasofu [44]
The papers with * are referenced in this paper.

(Due to the large number of references cited above in the text and in Table 3, they will not be listed here. See References, page 39.)

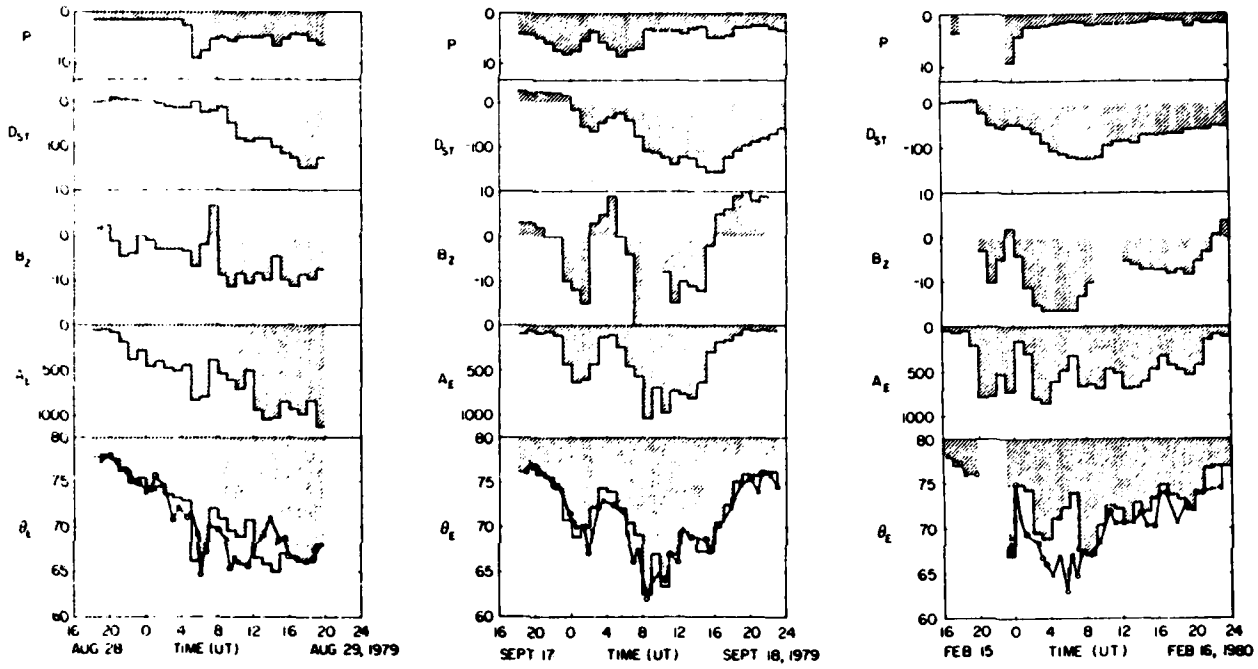

Figure 6. (Top panels) Hourly average of solar wind ram pressure ($\times 10^{-8}$ dyn cm^{-2}) from ISEE3. (Second panels) Hourly average Dst (γ). (Third panels) Hourly average of interplanetary B_Z component (γ). Note that the B_Z time base has not been offset to allow for solar wind transit time between the satellite and the magnetopause (~1 hour). (Fourth panels) Hourly average of AE index (γ). (Lower panels) Position of equatorial boundary of dayside cusp precipitation as measured by DMSP satellites in the northern (crosses) and southern (open circles) hemispheres, from Meng[24]. The histogram represents calculated latitude from the multiple linear regression equation (see Table A1), θ_E = 0.008 Dst - 0.54 P - 0.010 AE + 79.1, and the heavily shaded area is the difference between the measured and calculated values.

Perreault and Akasofu[45] have recently developed the parameter ϵ as a measure of the power generated by the solar wind-magnetosphere dynamo, drawn from Akasofu's theory that the kinetic energy eventually reaching the polar ionosphere is driven by the solar wind – IMF disposition and is not related to unloading processes internal to the magnetosphere. (This view is disputed by Schindler[46] and Heikilla.[47]) Perreault and Akasofu[45] define ϵ as

$$\epsilon = VB^2 \sin^4 \frac{\theta}{2} l_o^2$$

where V is the solar wind velocity, B is the magnitude of the IMF, l_o denotes the boundary of the magnetopause on the dayside (taken by Akasofu as fixed at 7 Re), and θ

$$= \tan^{-1} (B_y/B_z) \qquad B_z > 0$$

$$= 180 - \tan^{-1} (B_y/B_z) \quad B_z < 0 .$$

Baker et al[23] and Meloni et al[43] performed cross correlation analysis of the various solar wind quantities, including ϵ, with the Ae index. Baker's results are shown in Figure 7 and give information on the lead times between surges of southward B_z and resulting Ae behavior. Meloni's correlations of solar wind parameters vs Ae are presented in Table 4. Meloni's correlation differ from Baker's in the fact that they consider correlations of Ae with ϵ for all B_z (southward and northward) as well as correlations of Ae with ϵ for southward B_z.

---

45. Perreault, P., and Akasofu, S.-I. (1978) A study of geomagnetic storms, Geophys. J.R. Astron. Soc., 54:547.
46. Schindler, K. (1976) Solar Physics, 47:91.
47. Heikkila, W.F. (1983) The reason for magnetospheric substorms and solar flares, Solar Physics, 88:329-336.

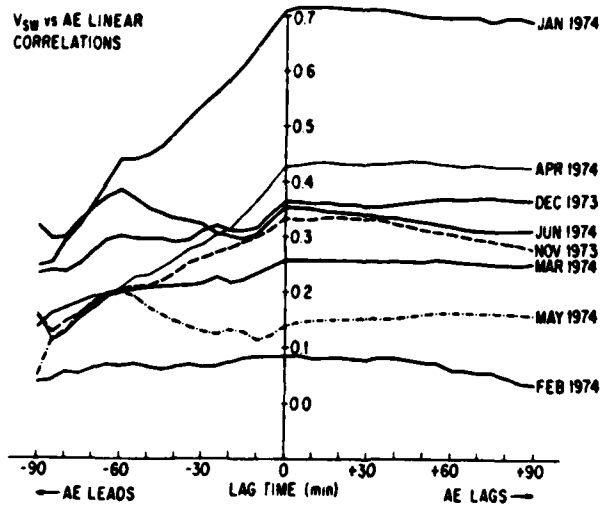

Figure 7a. Correlations of the AE Index With Solar Wind Velocity Shown Independently for Data Acquired in Individual Months From November 1973 Through June 1974. The ordinate is the correlation coefficient and the abscissa is the number of minutes by which the AE samples lagged the solar wind velocity samples

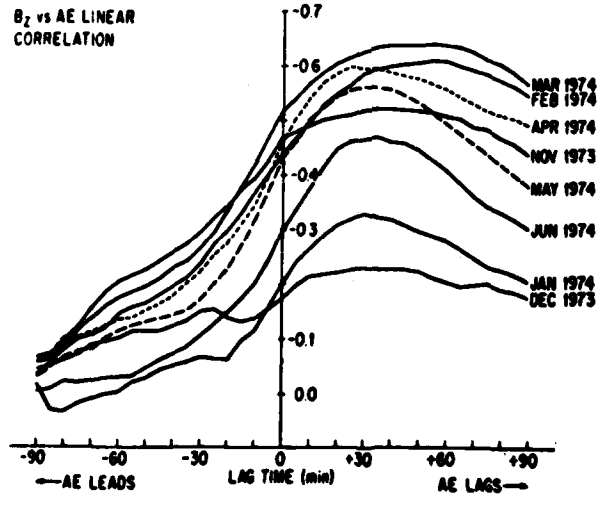

Figure 7b. Correlations of the AE Index With the GSM z-Component of the Interplanetary Magnetic Field

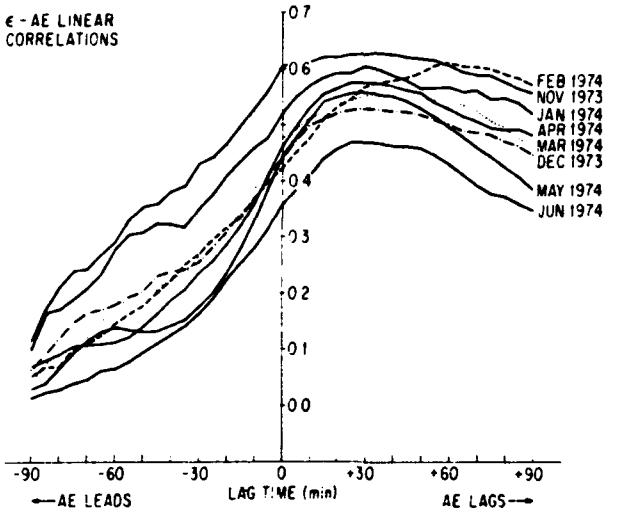

Figure 7c. Correlations of the AE Index With the Function ϵ (see text for definition of ϵ)

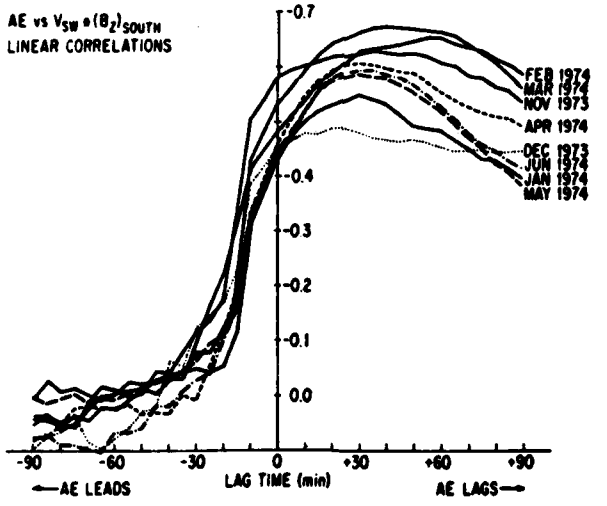

Figure 7d. Correlations of the AE Index With the Product of Solar Wind Velocity and B_z (GSM) South

Table 4. Summary of the Cross Correlation Coefficients Obtained in the Five Magnetic Storm Intervals for Contemporary Values of AE and Interplanetary Parameters and for the 1-h Delay in AE, for Data During All B_z Values and for Data During Only B_z South Values

	3-10 NOV '73		22-29 JAN '74		16-23 APR '74		7-14 JUN '74		3-10 JUL '74		
	AE	AE(+1)	AE	AE(+1)	AE	AE(+1)	AE	AE(+1)	AE	AE(+1)	
log ϵ	0 32	0 29	0 52	0 60	0 51	0 50	0 37	0 47	0 47	0 52	ALL B_z
$SIN^4 \frac{\theta}{2}$	0 44	0 43	0 32	0 35	0 28	0 34	0 60	0 68	0 65	0 73	
B_z	-0 38	-0 47	-0 36	-0 45	-0 35	-0 43	-0 58	-0 70	-0 68	-0 74	
$V \cdot B_z$	-0 40	-0 46	-0 40	-0 47	-0 45	-0 51	-0 61	-0 72	-0 65	-0 70	
log ϵ	0 58	0 64	0 72	0 70	0 66	0 68	0 61	0 69	0 62	0 63	ONLY B_z SOUTH
$SIN^4 \frac{\theta}{2}$	0 43	0 37	0 07	0 05	0 18	0 18	0 32	0 39	0 49	0 55	
B_z	-0 38	-0 52	-0 25	-0 33	-0 27	-0 30	-0 49	-0 67	-0 64	-0 68	
$V \cdot B_z$	-0 49	-0 60	-0 44	-0 49	-0 49	-0 49	-0 59	-0 78	-0 60	-0 62	
ϵ	0 58	0 63	0 53	0 53	0 56	0 55	0 53	0 63	0 35	0 28	

3.3 The Equatorward Boundary of the Auroral Oval

3.3.1 OBSERVATIONS OF THE RELATIONSHIP OF THE EQUATORWARD BOUNDARY TO THE DISCRETE AURORAL REGIONS

The auroral oval can be thought of as the projection of the plasma sheet onto the polar ionosphere. Figure 8 shows geometry of the earth and plasma sheet within the magnetosphere. The electrons and protons originating in the magnetospheric tail (below and to the right in the figure) are driven by the cross tail electric field toward auroral latitudes along the magnetic field lines in the plasma sheet.

Satellite observations in the early 70's indicated that there were two types of auroras that occurred: diffuse and discrete. Aboard the ISIS-2 satellite Lui et al[48] analyzed simultaneous measurements from a soft particle spectrometer, energetic

48. Lui, A.T.Y., Venkatesan, D., Anger, C.D., Akasofu, S.-I., Heikkila, W.J., Winningham, J.D., and Burrows, J.R. (1977) Simultaneous observations of particle precipitations and auroral emissions by the ISIS-2 Satellite in the 19-24 MLT Sector, J. Geophys. Res., 82:2210.

particle detectors and an auroral scanning photometer. The data showed that the diffuse auroras (< 1 Kr) tended to occur in what Winningham[49] referred to as the central plasma sheet and the discrete auroras corresponded to what was referred to as the boundary plasma sheet.

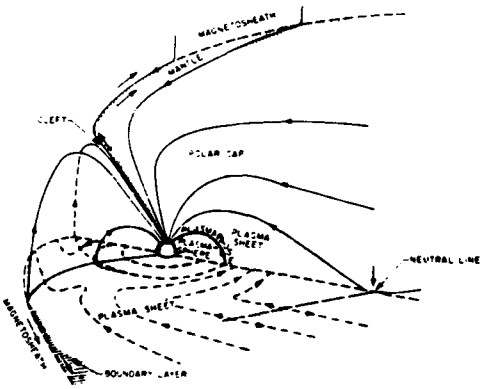

Figure 8. Sketch of Magnetic-Field Lines and Various Plasma Regions of the Magnetosphere. Only the northern dusk quadrant is shown for simplicity. Also drawn are contours denoting the flow or convection of plasma in the equatorial plane. All magnetic-field lines shown in this figure except the two near the dusk meridian lie completely in the noon-midnight meridian plane. The Van Allen radiation belts lie within and just beyond the plasmasphere

The discrete auroras were found to be em bedded within but often in the poleward half of the diffuse aurora. Figure 9 shows the relationship for quiet and substorm times.

---

49. Winningham, J.D., Yasuhara, F., Akasofu, S.-I., and Heikkila, W.J. (1975) The latitudinal morphology of 10 eV to 10 KeV electron fluxes during magnetically quiet and disturbed times in the 2100-0300 MLT sector, J. Geophys. Res., 80:3148.

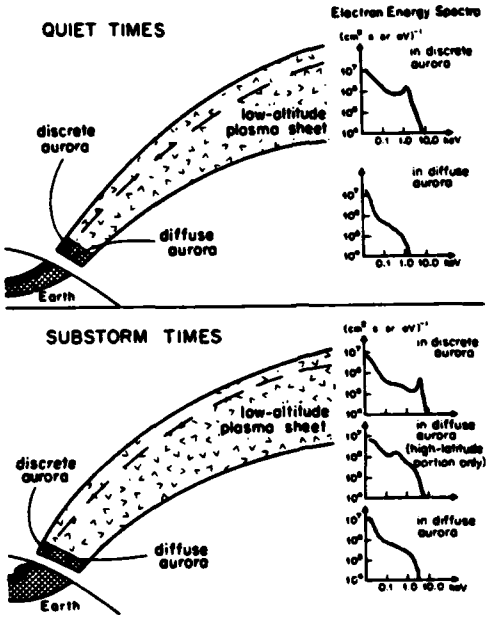

Figure 9. Schematic Diagram to Illustrate the Spatial Relationship Between the Plasma Sheet and the Two Types of Aurora. Characteristics of electron differential energy spectra in both types of aurora for quiet and substorm times are also illustrated (Lui et al[48])

Lui et al[48] looked at three kinds of auroras: those with diffuse auroras, those with bright arcs but no substorm and those with substorms, noting the boundaries of the diffuse and the discrete regions as well as K_p. These results are shown in Figure 10 and Table 5. This data suggests that if the equatorward boundary of the diffuse aurora is known, along with the amount of magnetic activity, the location of the region of discrete forms could be estimated.

A similar analysis of the relationship of the discrete and diffuse equatorward boundaries had also been measured by Nagata et al[50] in the southern hemisphere. These results are shown in Figure 11.[50]

50. Nagata, T., Kirasawa, T., and Ayakawa, M. (1975) Discrete and diffuse auroral belts in Antarctica, in Report of Ionosphere and Space Research in Japan, 29:149-152.

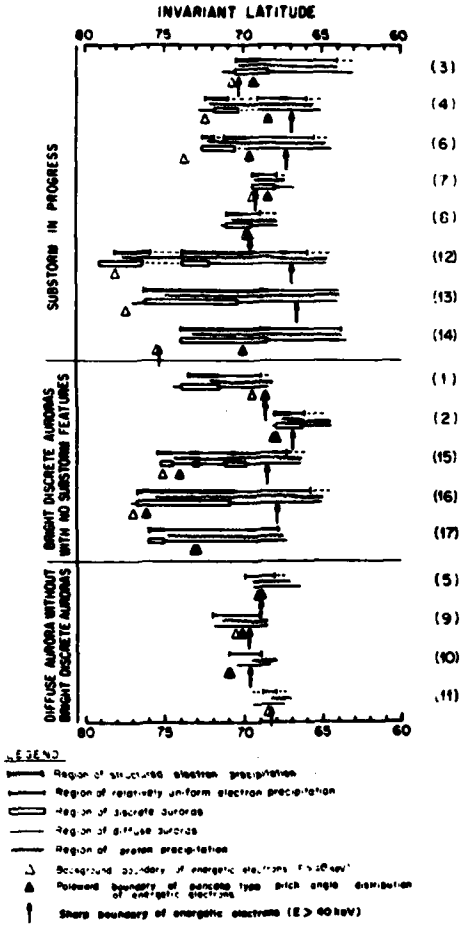

Figure 10. Schematic Diagram to Summarize the Results of Comparison Between Regions of Auroras and Particle Precipitation. Each pass is represented by three lines to indicate the extent and characteristics of particle precipitation and the types of aurora. Precipication and auroral emissions in the polar cap are not included. The numbers on the right side identify the events as given in Table 5

Table 5. Passes Selected for the Comparison of Measurements on Particle Precipitation and Auroral Intensity by Experiments on Board the Isis 2 Satellite

No.	Date	Time Interval of Passes	Kp*	MLT of Projected Path	Category of Auroral Activity
1	Dec. 11, 1971	0520-0534	0o	22.1	B
2	Dec. 12, 1971	0404-0417	1o	23.1	B
3	Dec. 13, 1971	0248-0303	3+	23.4	A
4	Dec. 13, 1971	0442-0457	2+	22.7	A
5	Dec. 14, 1971	0519-0533	1-	21.8	C
6	Dec. 15, 1971	0209-0221	2o	23.5	A
7	Dec. 16, 1971	0247-0301	0+	23.3	A
8	Dec. 16, 1971	0440-0456	0+	21.4	A
9	Dec. 20, 1971	0325-0339	0o	22.4	C
10	Dec. 20, 1971	0518-0532	0o	21.8	C
11	Dec. 21, 1971	0208-0222	1+	22.9	C
12	Dec. 22, 1971	0440-0456	3+	21.1	A
13	Dec. 26, 1971	0323-0340	4-	21.6	A
14	Jan. 4, 1972	0322-0339	3o	20.6	A
15	Jan. 10, 1972	0321-0336	1o	19.7	B
16	Jan. 11, 1972	0359-0415	4+	19.0	B
17	Jan. 11, 1972	0551-0605	4+	18.5	B

*The Kp values are taken from the 3-hour interval containing the end times of the passes.

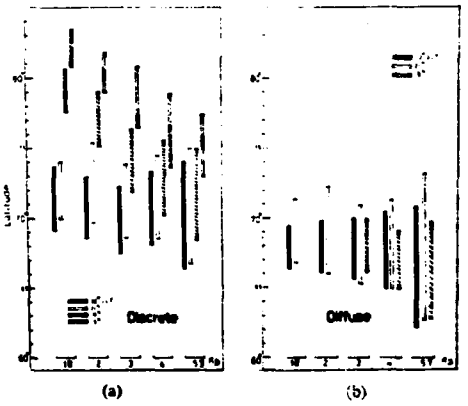

Figure 11. Average Locations of the Poleward and Equatorward Boundaries of the Discrete Auroral Belt (a) and the Diffuse One (b) as Dependent on Geomagnetic K_p Index and the Geomagnetic Local Time

Spiro et al[51] examined data from the Atmospheric Explorer C and D satellites and concluded that regions of the most intense precipitation corresponded to regions where upward field aligned currents are typically observed by satellite magnetometers.

51. Spiro, R.W., Reiff, P.H., and Maher, L.J., Jr. (1982) Precipitating electron energy flux and auroral zone conductances - an empirical model, J. Geophys. Res., 87:8215-8227.

Figure 12 shows the current flow at auroral altitudes. The currents are typically found near the poleward edge of the evening auroral zone for active geomagnetic conditions (Ae > 300 γ). With respect to local time distributions, Spiro concluded that: (1) the region of most intense precipitation for a given magnetic local time is located at higher latitudes in the premidnight sector than in the post midnight sector, and (2) for higher geomagnetic activity there is a tendency for the evening high latitude flux to extend into the early morning sector and the morning low latitude peak to extend westward into the late evening sector. Spiro's contours of precipitating energy flux are shown in Figure 13.

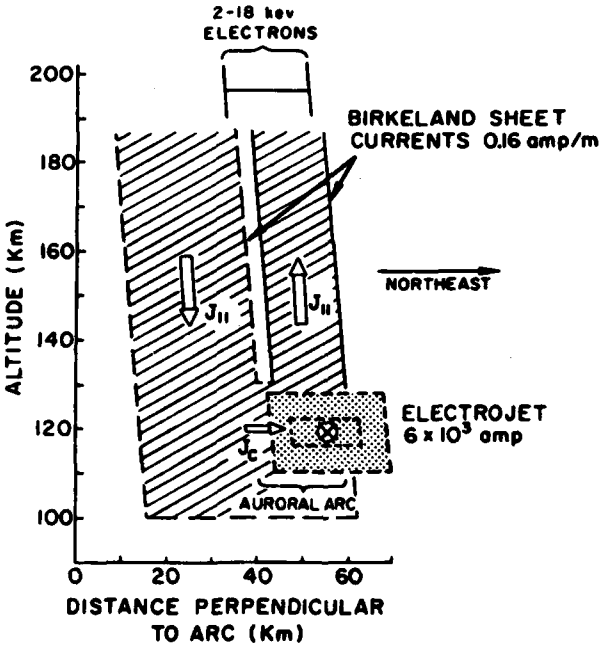

Figure 12. Model Current System for Auroral Arc as Fitted to Rocket Magnetometer Observations by Park and Cloutier (1971). The vertical currents of Figure 3.16A are assumed to be so remote as to produce a negligible effect (Courtesy of Journal of Geophysical Research; Copyright by American Geophysical Union)

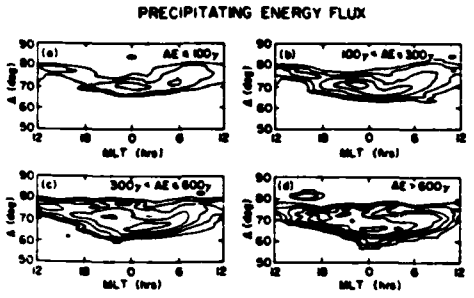

Figure 13. Contours of Constant Precipitating Electron Energy Flux Sorted According to Auroral Electrojet (AE) Index. The outermost contours correspond to a bin-average energy flux of 2.5×10^{-1} erg cm^{-2} s^{-1}, with adjacent contours representing factor of two increases in energy flux

Pinning down the specific location of the discrete events is difficult because of the rapid changes that can take place between successive satellite passes. Two or three satellites passing over the 2100-0300 sector can help considerably to monitor the locations of the discrete regions as the substorm progresses. Rostoker et al[52] describe the definition of this aspect of the substorm as follows:

> During this interval there may be a sequence of intensifications of the westward electrojet, each associated with a Pi 2 micropulsation burst and a westward travelling surge. As the substorm develops, the region of discrete auroras in the midnight sector expands poleward and westward (the poleward bulge). ..... The authors on the basis of their experience, feel that the magnetospheric substorm as defined above has a time scale of 1-3 hours.[4]

Sheehan's "fixed" auroral pattern (Sheehan[18]), suggests that a high inclination shuttle orbital track, which would be fixed with respect to the sun and passing over the midnight sector, could be able to monitor the progress of the substorm, considering the mirroring effect between the northern and southern ovals.

---

52. Rostoker, G., Akasofu, S.-I., Foster, J., Greenwald, R.A., Kamide, Y., Kawasaki, K., Lui, A.T.Y., McPherron, R.L., and Russell, C.T. (1980) Magnetospheric substorms - definition and signatures, J. Geophys. Res., 82(A4):1664.

3.3.2 MODELS CONCERNING THE LOCATION OF THE EQUATORWARD BOUNDARY

One of the earliest attempts to classify the equatorward boundary was by Feldstein and Starkov.[13] Using a broad network of all sky cameras from 61.6 to 75.3 degrees latitude, the oval was mapped every 15 min and correlated with the Q magnetic index. Their determination of both northern and southern boundaries as a function of local time and magnetic activity are shown in Figure 14.[53] These determinations have come to be known as the "classical" oval.

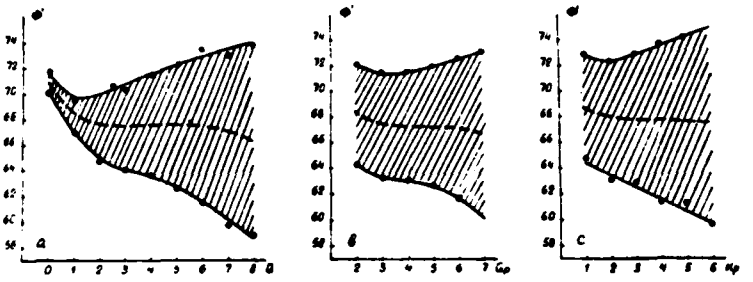

Figure 14. The Dependence of the Location of the Northern and Southern Edges of the Auroral Belt on the Indices (a) Q, (b) Q_v, and (c) K_p of Magnetic Activity Around Midnight (22-02 hours) in Local Geomagnetic Time. ϕ' is the corrected geomagnetic latitude. The dashed line represents the center line of the auroral belt

Eather[54] did extensive measurements of the equatorward boundary of the day-side aurora through the use of a keogram camera and found the boundary locations to be about 5° higher in latitude than Feldstein had found for Q = 0. The keogram measurements could be useful in characterizing the oval in general on a real time basis by relying on up to date modeling of the boundary. Computer codes have been developed that characterize the oval based on the input of a geomagnetic index (Comfort[55]). Such codes can be easily modified to accept a known location of the boundary for a particular MLT and characterize the rest of the oval based on how this location correlates with previous measurements that define the characterization.

---

53. Feldstein, Y.I., and Starkov, G.V. (1967) Dynamics of auroral belt and polar geomagnetic disturbances, Planet. Space Science, 15:209.

54. Eather, R.H. (1984) Dayside auroral dynamics, J. Geophys. Res., 89:1695-1700.

55. Comfort, R.H. (1972) Auroral Oval Kinematics Program, NASA Report CR-61373.

Gussenhoven et al[56] have modeled the location of the equatorward boundary for the whole oval based upon DMSP satellite measurements. The model accepts K_p as its input and determines the boundary from the equation

$$\Lambda = \Lambda_o + \alpha K_p$$

where Λ is the boundary predicted from the regression. Gussenhoven's tables of Λ_o and α are shown in Table 6.

Table 6. $\Lambda = \Lambda_o + \alpha K_p$

MLT	Number*	Λ_o	α	CC†
0000-0100	312	66.1	−1.99	−0.80
0100-0200	220	65.1	−1.55	−0.68
0400-0500	267	67.7	−1.48	−0.57
0500-0600	1123	67.8	−1.87	−0.71
0600-0700	2462	68.2	−1.90	−0.74
0700-0800	3159	68.9	−1.91	−0.76
0800-0900	2159	69.3	−1.87	−0.73
0900-1000	1178	69.5	−1.69	−0.66
1000-1100	864	69.5	−1.41	−0.57
1100-1200	513	70.1	−1.25	−0.52
1200-1300	353	69.4	−0.84	−0.35
1500-1600	63	70.9	−0.81	−0.34
1600-1700	204	71.6	−1.28	−0.66
1700-1800	526	71.1	−1.31	−0.69
1800-1900	997	71.2	−1.74	−0.82
1900-2000	2469	70.4	−1.83	−0.82
2000-2100	3309	69.4	−1.89	−0.82
2100-2200	3092	68.6	−1.86	−0.79
2200-2300	1482	67.9	−1.78	−0.77
2300-2400	461	67.8	−2.07	−0.81

*Number of boundaries used in each regression.
†Correlation coefficient.

Sauvaud et al[57] have come up with a model for the equatorward boundary in the 22-24 MLT sector based on the Ae index given by

56. Gussenhoven, M.S., Hardy, D.A., and Heinemann, N. (1983) Systematics of the Equatorward diffuse auroral boundary, J. Geophys. Res., 88:5692-5708.

57. Sauvaud, J.A., Crasnier, J., Galperin, Yu.I., and Feldstein, Y.I. (1983) A statistical study of the dynamics of the Equatorward boundary in the pre-midnight sector, Geophys. Res. Letts., 10:749-752.

$$\text{Inv. lat (deg)} = A + B \ln(\overline{Ae}) + C\,[\ln(\overline{Ae})]^2$$

with $\overline{Ae}$ being the average of Ae over various time intervals. The constants A, B and C are shown in Table 7 along with the square of the correlation (r^2) and the standard error (SE). The results indicate that the best fits occur when Ae is averaged over five hour intervals indicating that the boundary location depends mainly on the past magnetic activity.

Table 7. Result of the Fitting Procedure for Various Average AE Values

Averaging Period	A	B	C	r^2	SE
20 minutes	64.81	2.61	-0.54	0.77	1.67
2 hours	60.69	4.61	-0.78	0.81	1.53
3 hours	59.29	5.40	-0.88	0.86	1.33
5 hours	64.11	3.71	-0.75	0.90	1.13
10 hours	57.53	6.41	-1.02	0.75	1.74
20 hours	81.11	-3.54	0	0.61	2.09

3.4 Observations of Energetic Electron Intensity Changes at Geosynchronous Orbit

Studies of the relationship of evening/midnight sector electron dropouts at geosynchronous orbit (about 6.6 Re) to changes in the auroral electrojets offer exciting possibilities for the prediction of the onset of substorms (Erickson and Winckler[58], Erickson et al[59], and Sauvaud and Winckler[60]).

Studies of the behavior of energetic electrons (E >50 KeV) from ATS-1, ATS-5 and ATS-6 satellites in the evening and midnight sectors have shown that a pronounced decrease of energetic electron flux regularly precedes by about an hour the marked injection to synchronous orbit of hot plasma from the tail of magnetosphere

58. Erickson, K.N., and Winckler, J.R. (1973) Auroral electrojets and evening sector electron dropouts at synchronous orbit, J. Geophys. Res., 78:8373-8380.

59. Erickson, K.N., Swanson, R.L., Walker, R.J., and Winckler, J.R. (1979) A study of magnetosphere dynamics during auroral electrojet events by observations of energetic electron intensity changes at synchronous orbit, J. Geophys. Res., 84:931-942.

60. Sauvaud, J.A., and Winckler, J.R. (1980) Dynamics of plasma, energetic particles, and fields near synchronous orbit in the nighttime sector during magnetospheric substorms, Amer. Geophys. Union, Report No. 9A1592, pp. 2043-2056.

and simultaneous increase of the flux of the energetic particles. Coincident with the start of the electron decrease, a quiet arc system appears and intensifies as the decrease and field inflation continue (Erickson et al[59]). During some decreases, activity such as surges or brightenings may appear, but the major "breakup" always coincides closely with the expansion phase onset. Figure 15 is a representation of this process, which also correlates well with the variations of the electron flux.

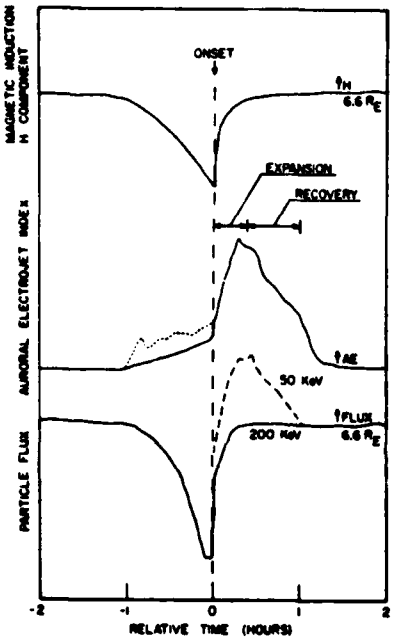

Figure 15. Schematic Representation of the Simultaneous Variations of the H Component of the Magnetic Induction at 6.6 R_E (antiparallel to the dipole axis), of the AE Index and of the Energetic Particle Flux at 6.6 R_E During a Substorm Preceded by a Quiet Period

Variations of electron fluxes and magnetic field variations for 22 November 1967 and 2 September 1967 aboard ATS-1 are shown in Figures 16 and 17, along with magnetometer traces for a number of ground stations. The Au and Al traces for the period are shown as well.

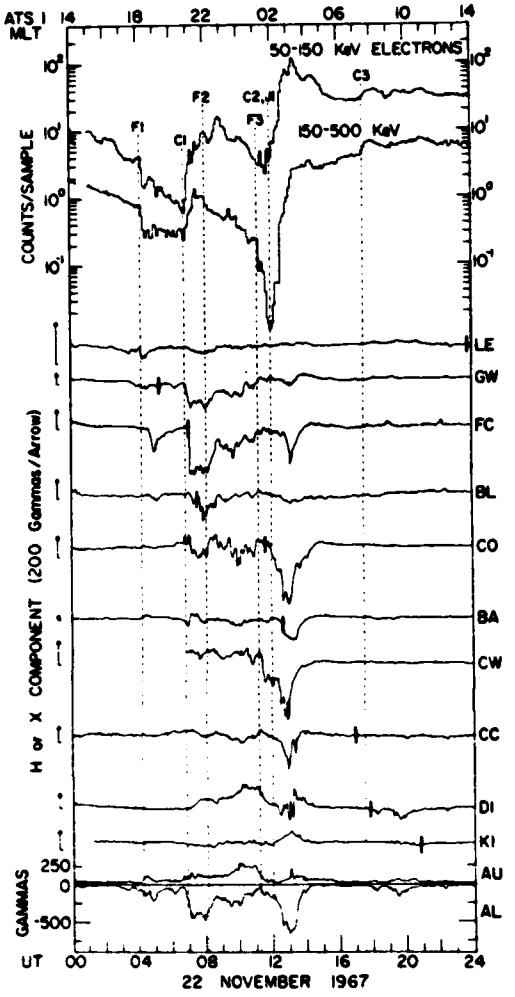

Figure 16. Average Electron Counts Over 6-min Intervals in Two Energy Channels for 22 November 1967. The AU and AL indices, magnetogram records, and time scales are as described for Figure 2

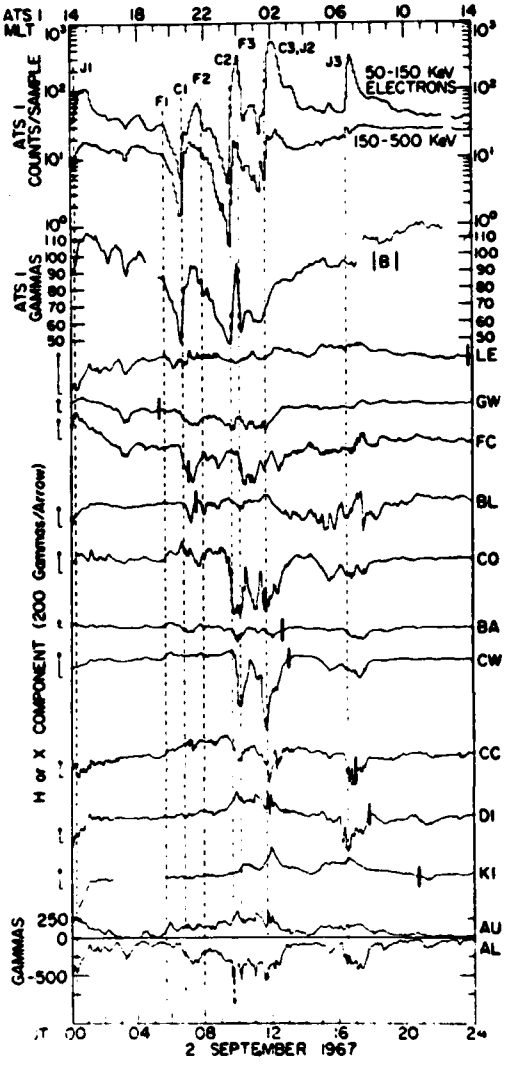

Figure 17. Average Electron Counts Over 6-min Intervals in Two Energy Channels for 2 September 1967. Local B, the AU and AL indices, magnetogram records, and time scales are as described for Figure 2

In the evening and near-midnight MLT regions, the decreases in flux of the 50-150 KeV, 150-500 KeV and 500-1000 KeV intervals have been shown to correlate with the change in the H component of the magnetic B field; that is, when the flux decreases, H decreases, and when the flux increases, H increases. In the morning sector, however, some large variations in the 50-150 KeV have been measured with no accompanied change in the B field. This type of electron flux increase has been attributed to the injection of plasma sheet particles near local midnight followed by their drift toward the east (Winckler;[61] Deforest and McIlwain[62]), where they arrive somewhat later than the more energetic fluxes (> 150 KeV) during the expansive phase of substorm. They follow morphological patterns that have been termed as "something different than a regular substorm" by McIlwain.[63] The location of the injection boundary of the plasma sheet particles at substorm onset has been derived by McIlwain[63] as

$$R_b = (122 - 10\,K_p) / (\phi - 73)$$

where R_b is the injection boundary position in the equatorial plane as a function of K_p and MLT in ϕ ($1800 \leq \phi \leq 2400$ CGLT).

Figure 18 shows the superpositioning of 161 traces of the Ae index, the 50-150 KeV fluxes, the 150-500 KeV fluxes, and the B field, which confirm the election decrease during the growth phase of the substorm.

The geographic location of a substorm can be roughly approximated with magnetic field line models. Erickson has successfully monitored the growth phase of the substorm by employing these field line models in combination with observations of the changes in the V component of the magnetic field aboard the GOES satellites.[5] At the present time, the GOES satellites have magnetometers that monitor the H and V components of the B field and this data is available real-time (Joselyn[64]).

---

61. Winckler, J.R. (1970) The origin and distribution of energetic electrons in the Van Allen radiation belt, Particles and Fields in the Magnetosphere, B.M. McCormac, Ed., D. Reidel, Dordrecht, Netherlands, p. 332.

62. Deforest, S.E., and McIlwain, C.E. (1971) Plasma clouds in the magnetosphere, J. Geophys. Res., 76:3587-3611.

63. McIlwain, C.E. (1975) Electron beams near the magnetic equator, Physics of the Hot Plasma in the Magnetosphere, Plenum, New York.

64. Joselyn, J.A., and Grubb, R.N. (1985) The Space Environment Monitors Onboard GOES, Report AIAA-85-0238, AIAA 23rd Aerospace Sciences Meeting, 14-17 January 1985, Reno, Nevada.

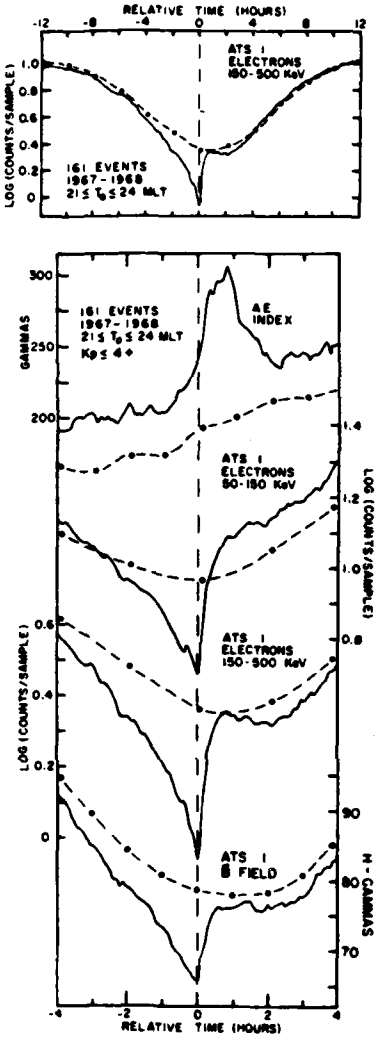

Figure 18. One Hundred Sixty-One Superposed Traces of AE Index, 50- to 150-keV and 150- to 500-keV Electron Counts and Magnetic Induction in the 2100-2400 MLT Bin, Selected From About 300 Days of Data With KP ≦ 4+. The heavy line shows the superposed epoch average for all 161 events in this local time bin. The dots with dashed lines indicate the background curve that was obtained by a superposition of all the 300 24-hour day intervals with Kp ≦ 4+. The start of each event (T = 0) was chosen at the onset time of the 150- to 500-keV electron count increase [from Swanson 1978]. The entire 24-hour period is shown in the upper panel for the same T = 0

3.5 Ground Based Observations

3.5.1 VISUAL ALL-SKY CAMERA AND PHOTOMETERS

All sky cameras are one of the most basic means to spot an aurora quickly while carrying on other ground measurements at the same time. Simultaneous all sky camera pictures from various ground stations can begin to piece together the

substorm puzzle. The sequence of all sky pictures shown in Figure 19 (Reference 65) from several meridian chain stations show a considerably better picture of the substorm phase than one picture does. Unfortunately, little has been accomplished to establish a central facility that could simultaneously monitor all sky camera pictures from all ground stations on a real-time basis, although this has been done semi-real-time from aircraft flying along the oval.

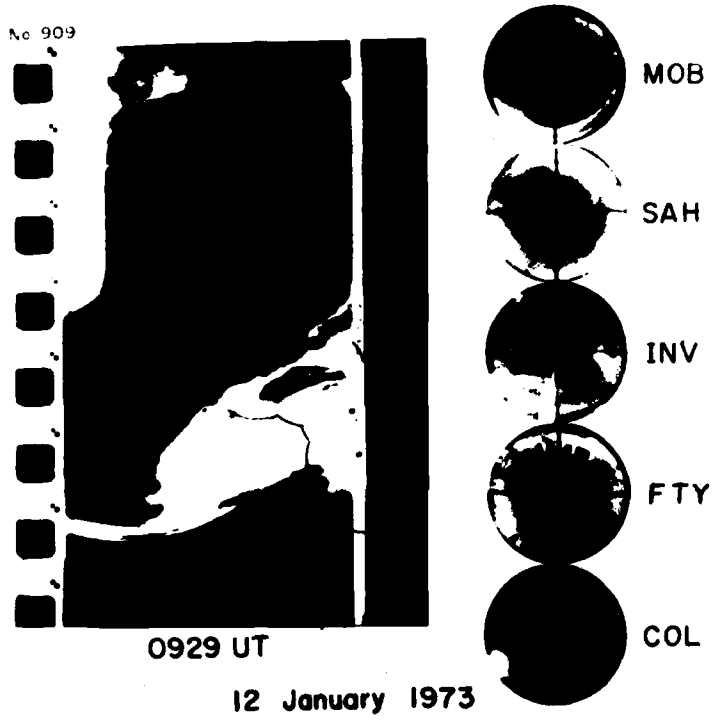

Figure 19. DMSP Photograph (orbit 909) and the Corresponding All-Sky Photographs From the Alaskan Meridian Chain of Stations; 12 January 1973

Photometer measurements are a useful means of quantifying the auroral intensities beyond using just an all-sky camera as they can individually monitor the different constituents (green at 5577 Å, red at 6300 Å, violet at 3914 Å, and so on).

---

65. Akasofu, S. -I. (1974) A study of auroral displays photographed from the DMSP-2 satellite and from the Alaska meridian chain of stations, in Space Science Reviews, 16:617-725.

The relative amounts of the constituents identify different types of aurorae which may have different morphological patterns.

3.5.2 GROUND BASED MAGNETOMETER TRACES

Ground based magnetometer traces are invaluable for identifying a geomagnetic disturbance in the vicinity of a station and are much more useful than the Kp index in monitoring geographically the phase of the substorm. Most stations record the H, D and Z traces which are the components of the total magnetic force field. Figure 20 shows the geometry. A thorough discussion of the interpretation of the H, D and Z component traces is given by Rostoker et al.[52] Figure 21 shows a general example of how these traces are interpreted.

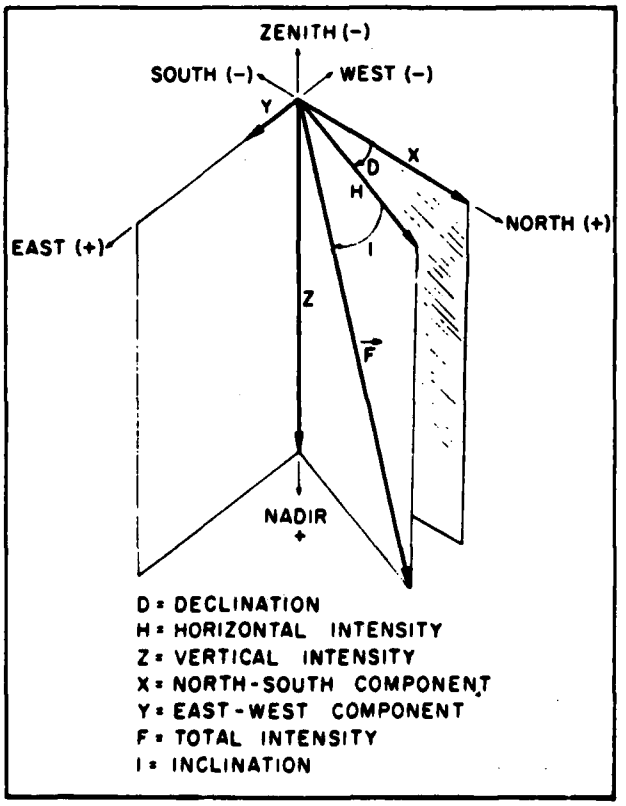

Figure 20. The Magnetic Force, F, and the Elements of the Earth's Magnetic Field

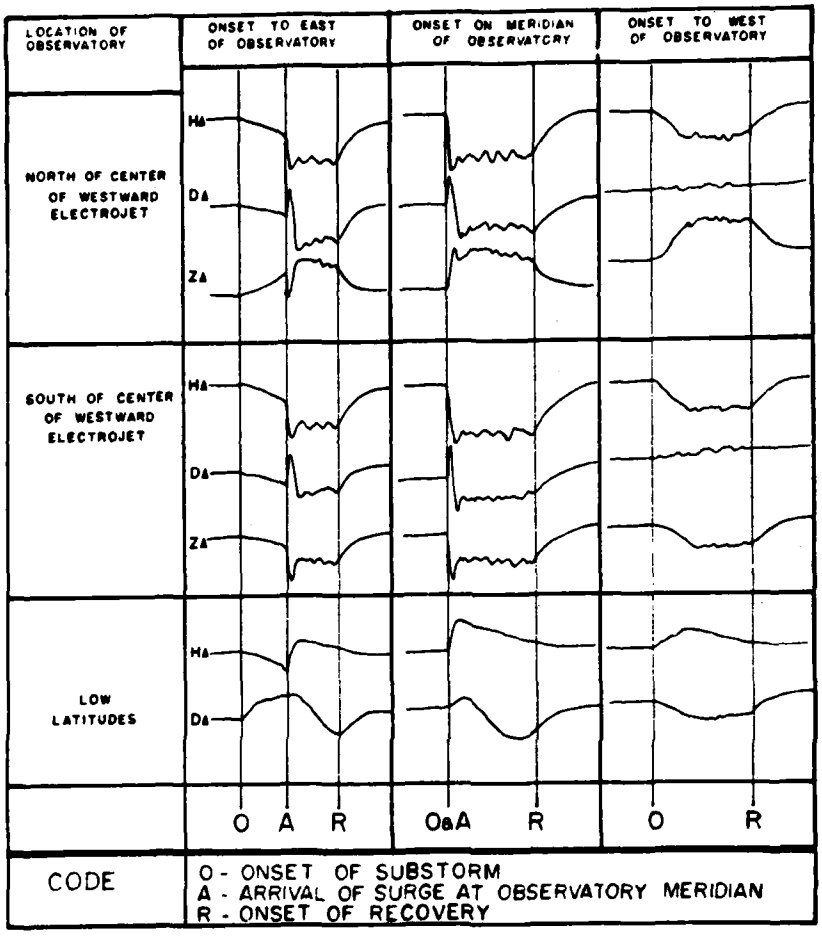

Figure 21. Schematic Representation of Magnetograms From Various Sites Placed at Different Positions With Respect to the High-Latitude Substorm Current Systems. These synthetic records can be compared with real data to establish the position and time sequence of events for an interval of substorm activity. Typical deflections at high-latitude observations range from ~ 100 to 1000 nT, while typical deflections at low-latitude stations range from a few nanoteslas to a few tens of nanoteslas

The importance of numerous stations becomes obvious upon examination of one component trace from a number of stations along a meridian chain. An example of a "stackplot"—the superpositioning of the traces of several stations on

top of one another—is shown in Figure 22 (see Reference 66). Such chains are able to monitor the expansion and contraction of the oval, and pinpoint the intensity and width of the westward or eastward electrojets.

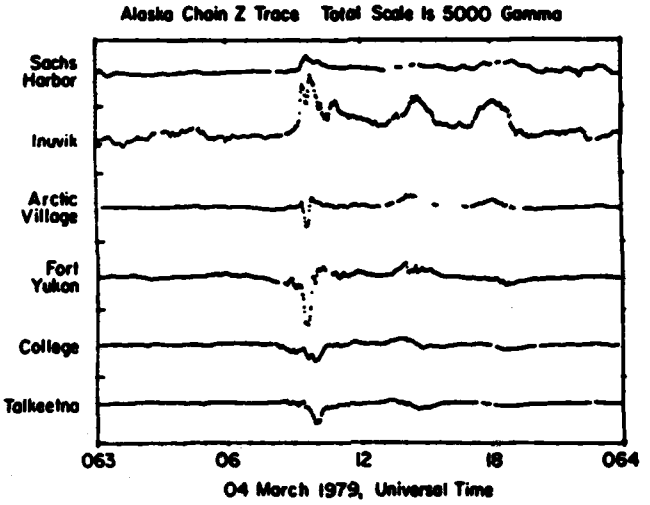

Figure 22. Stackplot of the Z Trace From the Alaskan IMS Magnetometer Chain, Illustrating a Substorm Signature Near 0900 UT

3.5.3 COORDINATED GROUND-SATELLITE AND AURORAL RADAR MEASUREMENTS

An important phenomenon to be considered with regard to the onset of a substorm is the Harang Discontinuity. The Harang Discontinuity is a thin strip, roughly aligned from east to west, which separates the eastward and westward electrojets, and its behavior is strongly dependent on magnetic activity. It is generally recognized that the first brightening arcs of a substorm onset usually occur in the vicinity of the Harang Discontinuity (Heppner;[67] Nielsen and Greenwald[68]).

---

66. Joselyn, J. A. et al (1982) SESC Geomagnetic Prediction, in Proceedings Workshop on Satellite Drag (NOAA/Space Environment Laboratory, Boulder, Colorado, p. 135.

67. Heppner, J. P. (1972) The Harang discontinuity in auroral belt ionospheric currents, Geophys. Publ., 29:105.

68. Nielsen, E., and Greenwald, R. A. (1979) Electron flow and visual aurora at the Harang discontinuity, J. Geophys. Res., 84:4189-4200.

Nielsen and Greenwald[68] have examined the Harang Discontinuity using the STARE (Scandinavian Twin Auroral Radar Experiment) and present ionosphere electron drift patterns which were associated with auroral arcs seen by all sky cameras (see Figure 23). They noted that for high magnetic activity prior to the substorm the discontinuity surged equatorward with a mean speed of 190 m/sec to be terminated by the sudden activation of an arc in the discontinuity, followed by a poleward expansion at substorm onset. The arcs tend to form just poleward of the discontinuity and diffuse aurorae tend to occur equatorward of it. Heppner[69] and Maynard[70] have also investigated the dynamics of the discontinuity.

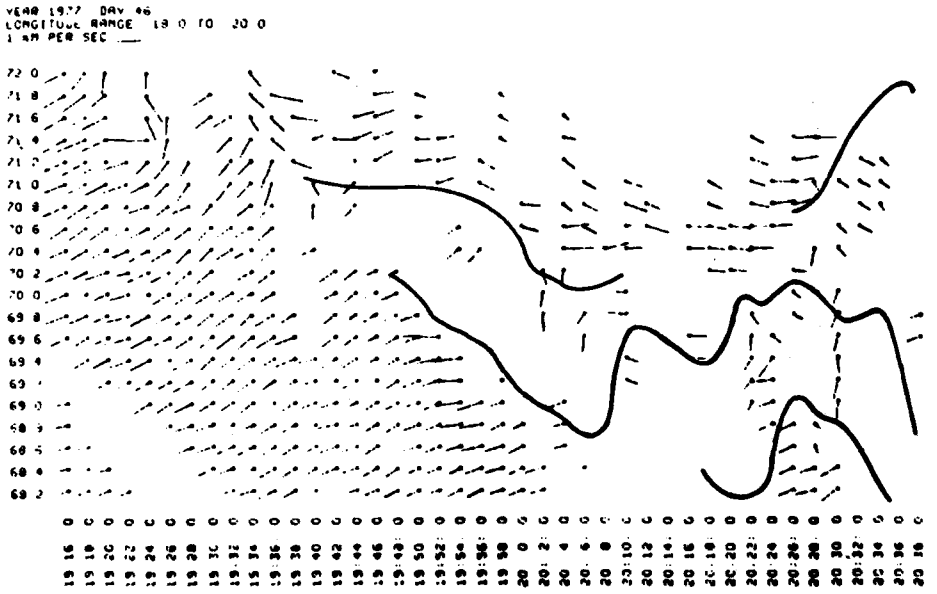

Figure 23. The Temporal Evolution of the Electron Drift Velocities During High Magnetic Activity. Note the equatorward motion of the Harang discontinuity. In this case, auroral arcs were located near the poleward and equatorward borders of the discontinuity

69. Heppner, J. P. (1976) Aurora and Airglow, B. M. McCormac, Ed., Reinhold, New York, p. 75.

70. Maynard, N. C. (1974) Electric field measurements across the Harang discontinuity, J. Geophys. Res., 79:4620.

Kamide and Akasofu[71] found the Harang Discontinuity to be the boundary between upward and downward field aligned currents. They investigated the relationship of field aligned currents and auroral arcs by comparing all sky pictures with the magnetometer measurements on board the Triad satellite and concluded that: (1) in the evening sector, discrete arcs are in general associated with upward aligned field currents and (2) no discrete arcs are associated with downward field-aligned currents. Figure 24 shows the Triad magnetometer traces and corresponding all sky pictures for a period when the satellite passed over the Harang Discontinuity, (shown at the Station Inuvik on the map).

3.5.4 RIOMETER MEASUREMENTS

A riometer measures the absorption of cosmic radiation. Riometer measurements can give indications of particle influx prior to a substorm. Weber et al[72] noted the increase of riometer absorption for several hours prior to a sudden substorm commencement on 4 August 1972. In general, during the austral winter of 1972, Weber et al's observations of absorption increases were associated with substorms.

---

71. Kamide, Y., and Akasofu, S. -I. (1976) The location of the field-aligned currents with respect to discrete auroral arcs, J. Geophys. Res., 81:3999-4003.

72. Weber, E.J., Mende, S.B., and Eather, R.H. (1976) Optical diagnostics August 1972 PCA Event, J. Geophys. Res., 81:5479-5487.

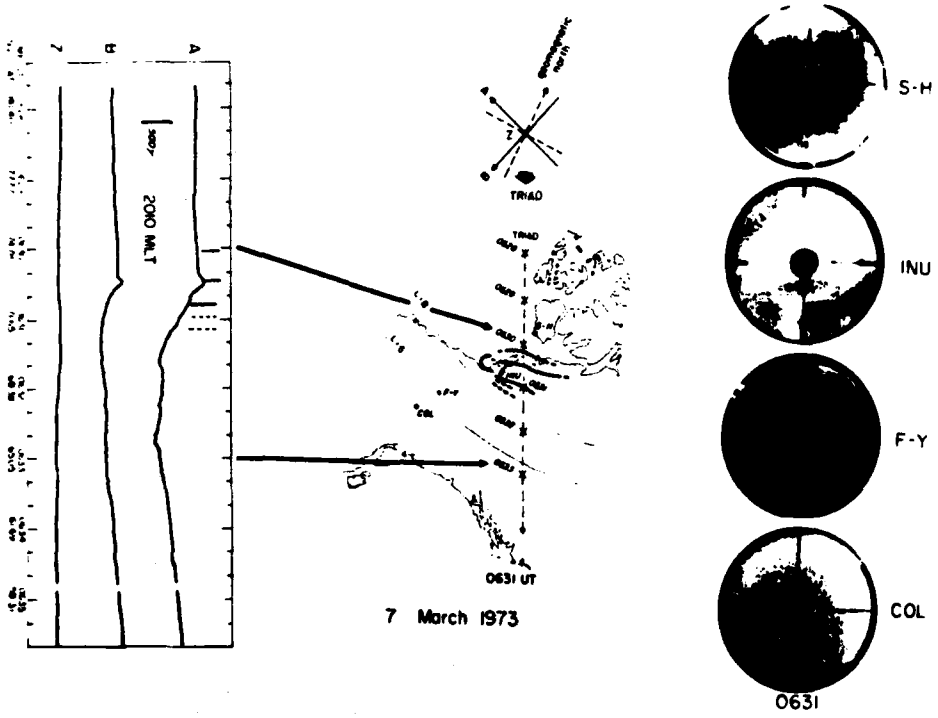

Figure 24. Triad Magnetometer Data in the A, B, and Z Coordinates (fixed with respect to the satellite trajectory), the Satellite Pass Over Alaska Together With the Locations of Auroras, and the All-Sky Camera Photographs Taken From a Chain of Four Alaska Meridian Stations, Sachs Harbour (Λ = 76.16°), Inuvik (70.98°), Fort Yukon (66.83°), and College (64.63°) at 0631 UT on 7 March 1973. Less-bright arcs are shown by dashed lines

References

1. Chamberlain, J.W. (1961) Physics of the Aurora and Airglow, Academic Press, New York.
2. Gneryshev, M.N. (1977) Essential features of the 11-year solar cycle Solar Physics, 51:175-183.
3. Timothy, A.F., Krieger, A.S., and Vaiana, G.S. (1975) Solar Physics, 42:135.
4. Mayaud, P.N. (1980) Derivation, meaning and use of geomagnetic indices, American Geophysical Union, Geophysical Monograph 22, Washington, D.C.
5. Sargent, H.H. (1985) Recurrent geomagnetic activity: evidence for long-lived stability in solar wind structure, in J. Geophys. Res., 90:1425-1428.
6. Mayaud, P.N. (1973) A hundred year series of geomagnetic data 1868-1967, IAGA Bull. Vol. 33.
7. Suess, S.T. (1979) Models of coronal hole flows, Space Science Review, 23:159-200.
8. Sheeley, N.R., Harvey, J.W., and Feldman, W.C. (1976) Coronal holes, solar wind streams, and recurrent geomagnetic disturbances: 1973-1976, Solar Physics, 49:271-278.
9. Koomen, M.J., and Howard, R.A. (1974) Solar Physics, 37:469.
10. Hargreaves, J.K. (1979) The Upper Atmosphere and Solar Terrestrial Relations, (Van Nostrand Reinhold Co., New York).
11. Newton, H.W. (1943) Solar flares and magnetic storms, Monthly No. Roy. Ast. Soc. 103:244-257.
12. Newton, H.W., and Jackson, W. (1951) Observational aspect of solar corpuscular radiation, in C.I.U.S. Septieme Rapport de la Commission pour l'Etude des Relations entre les Phenomenes Solaires et Terrestres, Hemmerle, Pettit et Cie, Paris.
13. Dodson, H.W., and Hedeman, E.R. (1958) Geomagnetic disturbances associated major premaximum bursts at radio frequencies ≤ 200 Mc/s, J. Geophys. Res., 63:77-96.

14. Krivsky, L. (1977) Important flare events in variations of the auroral electrojet index, Studia Geoph. et Geod. 21:410-414.

15. Sheehan, R.E., Carovillano, R.L., and Gussenhoven, M.S. (1982) Occurrence and recurrence in auroral activity in DMSP images, J. Geophys. Res. 87(No. A3):3581-3589.

16. Akasofu, S.-I. (1968) Polar and Magnetospheric Substorms, D. Reidel, Hingham, Massachusetts.

17. Carovillano, R.L., Siscoe, G.L., Sheehan, R.E., Eather, R.H., and Gussenhoven, M.S. (1975) Unified Model of Auroral Substorm Development, AFCRL-TR-75-0558, AD A020313.

18. Sheehan, R.E. Ph. D. Thesis (Boston College, 1977), p. 182.

19. Dungey, J.W. (1961) Interplanetary magnetic field and the auroral zones, Phys. Rev. Letters, 6:47.

20. Eather, R.H., Mende, S.B., and Weber, E.J. (1979) Dayside aurora and relevance to substorm current systems and dayside merging, J. Geophys. Res., 84:3339.

21. Eather, R.H. (1985) Polar cusp dynamics, J. Geophys. Res., 90:1569-1576.

22. Kamide, Y., and Akasofu, S.-I. (1982) Total current of the auroral electrojet estimated from the IMS Alaska meridian chain of magnetic observatories, Planet. Space Sci., 30:621.

23. Baker, D.N., Hones, E.W., Jr., Payne, J.B., and Feldman, W.C. (1981) A high time resolution of interplanetary parameter correlations with Ae, Geophysical Res. Lett., 8(No. 2):179-182.

24. Meng, C.I., Tsurutani, B., Kawasaki, K., and Akasofu, S.-I. (1973) Cross correlation analysis of the Ae index and the interplanetory magnetic field B_z component, J. Geophys. Res., 78:617.

25. Snyder, C.W., Neugebauer, M., and Rao, U.R. (1963) The solar wind velocity and its correlation with cosmic-ray variations and with solar and geomagnetic activity, J. Geophys. Res., 68:6361.

26. Olbert, S. (1968) in R.L. Carovillano, J.F. McClay, and H.R. Radoski, Eds., Physics of the Magnetosphere, D. Reidel Publ. Co., Dordrecht, Holland, p. 641.

27. Ballif, J.R., Jones, D.E., and Coleman, P.J., Jr. (1969) Further evidence on the correlation between transverse fluctuations in the interplanetary magnetic field and Kp, J. Geophys. Res., 74:2289.

28. Arnoldy, R.L. (1971) Signature in the interplanetary medium for substorms, J. Geophys. Res., 76:5189.

29. Bobrov, M.S. (1973) Kp index correlations with solar-wind parameters during the first and second stages of a recurrent geomagnetic storm, Planet. Space Sci., 21:2139.

30. Garrett, H.B., Hassler, A.J., and Hill, T.W. (1974) Influence of solar wind variability on geomagnetic activity, J. Geophys. Res., 79:4603.

31. Murayama, T., and Hakamada, K. (1975) Effects of solar wind parameters on the development of magnetospheric substorms, Planet. Space Sci., 23:75.

32. Burton, R.K., McPherron, R.L., and Russell, C.T. (1975) An empirical relationship between interplanetary conditions and Dst, J. Geophys. Res., 80:4204.

33. Crooker, N.U., Feynman, J., and Gosling, J.T. (1977) On the high correlation between long-term averages of solar wind speed and geomagnetic activity, J. Geophys. Res., 82:1933.

34. Svalgaard, L. (1977) Coronal Holes and High Speed Wind Streams, Colorado Associated University Press, Boulder, Colorado, p. 371.

35. Maezawa, K. (1979) Statistical study of the dependence of geomagnetic activity on solar wind parameters, in W.P. Olson, Ed., Quantitative Modeling of Magnetospheric Processes, American Geophysical Union, Washington, D.C., p. 436.

36. Holzer, R.E., and Slavin, J.A. (1978) Magnetic flux transfer associated with expansions and contractions of the dayside magnetosphere, J. Geophys. Res., 83:3831.

37. Murayama, T. (1979) in T. Obayashi, Ed., Magnetospheric Study 1979 Japanese IMS Committee, Tokyo, Japan, P. 296.

38. Murayama, T., Aoki, T., Nakai, H., and Hakamada, K. (1980) Empirical formula to relate the auroral electrojet intensity with interplanetary parameters, Planet. Space Sci., 28:803.

39. Lei, W., Gendrin, R., Higel, B., and Berchem, J. (1981) Relationships between the solar wind electric field and the magnetospheric convection electric field, Geophys. Res. Letts., 8(No. 10):1099.

40. Reiff, P.H., Spiro, R.W., and Hill, T.W. (1981) Dependence of polar cap potential drip on interplanetary parameters, J. Geophys. Res. 86(A9):7639.

41. Holzer, R.E., and Slavin, J.A. (1982) An evaluation of three predictors of geomagnetic activity, J. Geophys. Res., 87:2558.

42. Iijima, T., and Potemra, T.A. (1982) The relationship between interplanetary quantities and Birkeland current densities, Geophys. Res. Letts., 9(No. 4):442.

43. Meloni, A., Wolfe, A., and Lanzerotti, L.J. (1982) On the relationships between interplanetary quantities and the global auroral electrojet index, J. Geophys. Res., 87:119-127.

44. Akasofu, S.-I. (1983) Solar-wind disturbances and the solar wind magnetosphere energy coupling function, Space Science Review, 34:173-183.

45. Perreault, P., and Akasofu, S.-I. (1978) A study of geomagnetic storms, Geophys. J.R. Astron. Soc., 54:547.

46. Schindler, K. (1976) Solar Physics, 47:91.

47. Heikkila, W.F. (1983) The reason for magnetospheric substorms and solar flares, Solar Physics, 88:329-336.

48. Lui, A.T.Y., Venkatesan, D., Anger, C.D., Akasofu, S.-I., Heikkila, W.J., Winningham, J.D., and Burrows, J.R. (1977) Simultaneous observations of particle precipitations and auroral emissions by the ISIS-2 Satellite in the 19-24 MLT Sector, J. Geophys. Res., 82:2210.

49. Winningham, J. D., Yasuhara, F., Akasofu, S. -I., and Heikkila, W. J. (1975) The latitudinal morphology of 10 eV to 10 KeV electron fluxes during magnetically quiet and disturbed times in the 2100-0300 MLT sector, J. Geophys. Res., 80:3148.

50. Nagata, T., Kirasawa, T., and Ayakawa, M. (1975) Discrete and diffuse auroral belts in Antarctica, in Report of Ionosphere and Space Research in Japan, 29:149-152.

51. Spiro, R. W., Reiff, P. H., and Maher, L. J., Jr. (1982) Precipitating electron energy flux and auroral zone conductances - an empirical model, J. Geophys. Res., 87:8215-8227.

52. Rostoker, G., Akasofu, S. -I., Foster, J., Greenwald, R. A., Kamide, Y., Kawasaki, K., Lui, A. T. Y., McPherron, R. L., and Russell, C. T. (1980) Magnetospheric substorms - definition and signatures, J. Geophys. Res., 85(A4):1664.

53. Feldstein, Y. I., and Starkov, G. V. (1967) Dynamics of auroral belt and polar geomagnetic disturbances, Planet. Space Science, 15:209.

54. Eather, R. H. (1984) Dayside auroral dynamics, J. Geophys. Res., 89:1695-1700.

55. Comfort, R. H. (1972) Auroral Oval Kinematics Program, NASA Report CR-61373.

56. Gussenhoven, M. S., Hardy, D. A., and Heinemann, N. (1983) Systematics of the Equatorward diffuse auroral boundary, J. Geophys. Res., 88:5692-5708.

57. Sauvaud, J. A., Crasnier, J., Galperin, Yu. I., and Feldstein, Y. I. (1983) A statistical study of the dynamics of the Equatorward boundary in the pre-midnight sector, Geophys. Res. Letts., 10:749-752.

58. Erickson, K. N., and Winckler, J. R. (1973) Auroral electrojets and evening sector electron dropouts at synchronous orbit, J. Geophys. Res., 78:8373-8380.

59. Erickson, K. N., Swanson, R. L., Walker, R. J., and Winckler, J. R. (1979) A study of magnetosphere dynamics during auroral electrojet events by observations of energetic electron intensity changes at synchronous orbit, J. Geophys. Res., 84:931-942.

60. Sauvaud, J. A., and Winckler, J. R. (1980) Dynamics of plasma, energetic particles, and fields near synchronous orbit in the nighttime sector during magnetospheric substorms, Amer. Geophys. Union, Report No. 9A1592, pp. 2043-2056.

61. Winckler, J. R. (1970) The origin and distribution of energetic electrons in the Van Allen radiation belt, Particles and Fields in the Magnetosphere, B. M. McCormac, Ed., D. Reidel, Dordrecht, Netherlands, P. 332.

62. Deforest, S. E., and McIlwain, C. E. (1971) Plasma clouds in the magnetosphere, J. Geophys. Res., 76:3587-3611.

63. McIlwain, C. E. (1975) Electron beams near the magnetic equator, Physics of the Hot Plasma in the Magnetosphere, Plenum, New York.

64. Joselyn, J. A., and Grubb, R. N. (1985) The Space Environment Monitors Onboard GOES, Report AIAA-85-0238, AIAA 23rd Aerospace Sciences Meeting, 14-17 January 1985, Reno, Nevada.

65. Akasofu, S. -I. (1974) A study of auroral displays photographed from the DMSP-2 satellite and from the Alaska meridian chain of stations, in Space Science Reviews, 16:617-725.

66. Joselyn, J. A. et al (1982) SESC Geomagnetic Prediction, in Proceedings, Workshop on Satellite Drag (NOAA/Space Environment Laboratory, Boulder, Colorado, p. 135.

67. Heppner, J. P. (1972) The Harang discontinuity in auroral belt ionospheric currents, Geophys. Publ., 29:105.

68. Nielsen, E., and Greenwald, R. A. (1979) Electron flow and visual aurora at the Harang discontinuity, J. Geophys. Res. 84:4189-4200.

69. Heppner, J. P. (1976) Aurora and Airglow, B. M. McCormac, Ed., Reinhold, New York, p. 75.

70. Maynard, N. C. (1974) Electric field measurements across the Harang discontinuity, J. Geophys. Res., 79:4620.

71. Kamide, Y., and Akasofu, S.-I. (1976) The location of the field-aligned currents with respect to discrete auroral arcs, J. Geophys. Res., 81:3999-4003.

72. Weber, E. J., Mende, S. B., and Eather, R. H. (1976) Optical diagnostics of the August 1972 PCA Event, J. Geophys. Res., 81:5479-5487.

END

FILMED

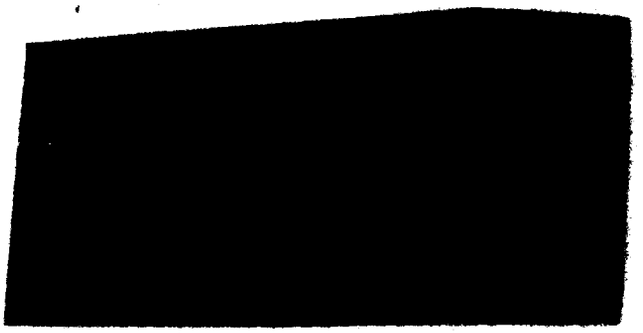

DTIC